Full humanization of the glycolytic pathway in Saccharomyces cerevisiae

Boonekamp, Francine J.; Knibbe, Ewout; Vieira-Lara, Marcel A.; Wijsman, Melanie; Luttik, Marijke A.H.; van Eunen, Karen; Ridder, Maxime den; Pabst, Martin; Daran, Jean Marc; Daran-Lapujade, Pascale

DOI
10.1016/j.celrep.2022.111010

Publication date
2022

Document Version
Final published version

Published in
Cell Reports

Citation (APA)
Boonekamp, F. J., Knibbe, E., Vieira-Lara, M. A., Wijsman, M., Luttik, M. A. H., van Eunen, K., Ridder, M. D., Pabst, M., Daran, J. M., & Daran-Lapujade, P. (2022). Full humanization of the glycolytic pathway in Saccharomyces cerevisiae. *Cell Reports*, *39*(13), 111010. Article 111010. https://doi.org/10.1016/j.celrep.2022.111010

Cell Reports

Article

Full humanization of the glycolytic pathway in *Saccharomyces cerevisiae*

Graphical abstract

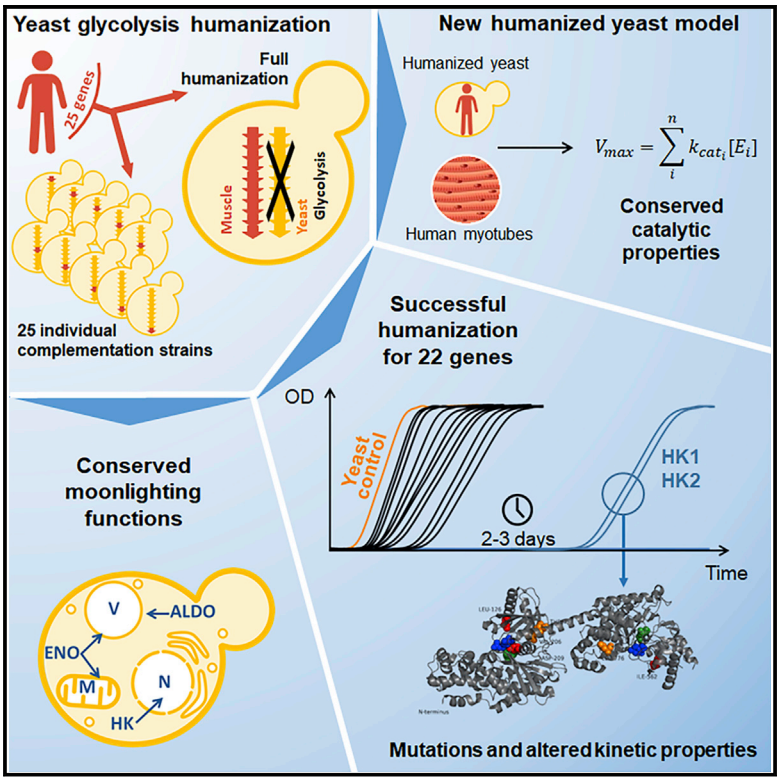

Highlights

- The entire yeast glycolytic pathway was successfully humanized
- All 25 tested human glycolytic genes, except *HK1–HK3*, complement their yeast ortholog
- Yeast and human glycolytic enzymes have well-conserved moonlighting functions
- Evolutionary optimization of human enzymes in yeast occurs at posttranscriptional level

Authors

Francine J. Boonekamp, Ewout Knibbe, Marcel A. Vieira-Lara, ..., Jean-Marc Daran, Barbara M. Bakker, Pascale Daran-Lapujade

Correspondence

p.a.s.daran-lapujade@tudelft.nl

In brief

By successfully humanizing an entire essential pathway in the model yeast *Saccharomyces cerevisiae*, Knibbe et al. demonstrate the remarkable conservation and replaceability of metabolic pathways between distant eukaryotes. The constructed humanized yeasts offer new models to study human glycolysis in a naive, simplified context.

Boonekamp et al., 2022, Cell Reports *39*, 111010
June 28, 2022
https://doi.org/10.1016/j.celrep.2022.111010

CellPress

Cell Reports

CellPress
OPEN ACCESS

Article

Full humanization of the glycolytic pathway in *Saccharomyces cerevisiae*

Francine J. Boonekamp,[1,5] Ewout Knibbe,[1,5] Marcel A. Vieira-Lara,[2] Melanie Wijsman,[1] Marijke A.H. Luttik,[1] Karen van Eunen,[2] Maxime den Ridder,[1] Reinier Bron,[3] Ana Maria Almonacid Suarez,[4] Patrick van Rijn,[3] Justina C. Wolters,[2] Martin Pabst,[1] Jean-Marc Daran,[1] Barbara M. Bakker,[2] and Pascale Daran-Lapujade[1,6,*]

[1]Department of Biotechnology, Delft University of Technology, Van Der Maasweg 9, 2629 Delft, the Netherlands

[2]Laboratory of Pediatrics, Section Systems Medicine and Metabolic Signalling, Center for Liver, Digestive and Metabolic Disease, University of Groningen, University Medical Center Groningen, Groningen, the Netherlands

[3]Department of Biomedical Engineering-FB40, W.J. Kolff Institute for Biomedical Engineering and Materials Science-FB41, University of Groningen, University Medical Center Groningen, Groningen, the Netherlands

[4]Department of Pathology and Medical Biology, University of Groningen, University Medical Center Groningen, Groningen, the Netherlands

[5]These authors have contributed equally

[6]Lead contact

*Correspondence: p.a.s.daran-lapujade@tudelft.nl

https://doi.org/10.1016/j.celrep.2022.111010

SUMMARY

Although transplantation of single genes in yeast plays a key role in elucidating gene functionality in metazoans, technical challenges hamper humanization of full pathways and processes. Empowered by advances in synthetic biology, this study demonstrates the feasibility and implementation of full humanization of glycolysis in yeast. Single gene and full pathway transplantation revealed the remarkable conservation of glycolytic and moonlighting functions and, combined with evolutionary strategies, brought to light context-dependent responses. Human hexokinase 1 and 2, but not 4, required mutations in their catalytic or allosteric sites for functionality in yeast, whereas hexokinase 3 was unable to complement its yeast ortholog. Comparison with human tissues cultures showed preservation of turnover numbers of human glycolytic enzymes in yeast and human cell cultures. This demonstration of transplantation of an entire essential pathway paves the way for establishment of species-, tissue-, and disease-specific metazoan models.

INTRODUCTION

Because of its tractability and genetic accessibility, *Saccharomyces cerevisiae* plays a key role as a simplified model organism for higher eukaryotes. Many discoveries in yeast-native processes, such as the cell cycle and ribosome biogenesis, were pivotal for understanding their mammalian equivalents (Nurse, 2002; Woolford and Baserga, 2013). In addition, yeast is used to study a wide range of diseases, such as cancer, diabetes, and neurodegenerative diseases (Petranovic and Nielsen, 2008). Heterologous expression of human genes in yeast enables detailed investigation of human biology and disease-specific variations of human genes (Laurent et al., 2016). Because the yeast and human genomes share over 2,000 groups of orthologs (Laurent et al., 2016), several large initiatives have explored the complementarity of human genes in yeast and shown a high degree of functional conservation (Garge et al., 2020; Hamza et al., 2015, 2020; Kachroo et al., 2015; Laurent et al., 2016, 2020; Sun et al., 2016; Zhang et al., 2003). These studies are, however, complicated by the genetic redundancy of eukaryotic genomes (Prince and Pickett, 2002), particularly for genes encoding proteins with metabolic functions (Steinke et al., 2006; Gordon et al., 2009).

Although individual gene complementation in yeast is an interesting approach to characterize single human proteins, humanization of entire pathways or processes would greatly increase the usefulness of yeast models. Such "next-level" models can capture the native functional context of the humanized proteins and enable study of more complex, multigene phenotypes and epistatic gene interactions. The feasibility of such extensive humanization projects depends largely on the replaceability of yeast genes by their human orthologs. Recent large-scale humanization and bacterialization efforts of the yeast genome suggested that replaceability was better predicted on a pathway or process basis than by sequence conservation (Kachroo et al., 2015, 2017). To date, reports of full humanization of pathways or protein complexes are scarce (Agmon et al., 2020; Garge et al., 2020; Hamilton and Zha, 2015; Labunskyy et al., 2014; Truong and Boeke, 2017). However, rapid developments in synthetic biology have tremendously increased our ability to extensively remodel microbial genomes and promise to bring more examples of large-scale humanization in the future.

The Embden-Meyerhof-Parnas pathway of glycolysis, nearly ubiquitous in eukaryotes, has a central role in carbon metabolism and is involved in a wide range of diseases in mammals, including cancer, with the well-known Warburg effect (Warburg,

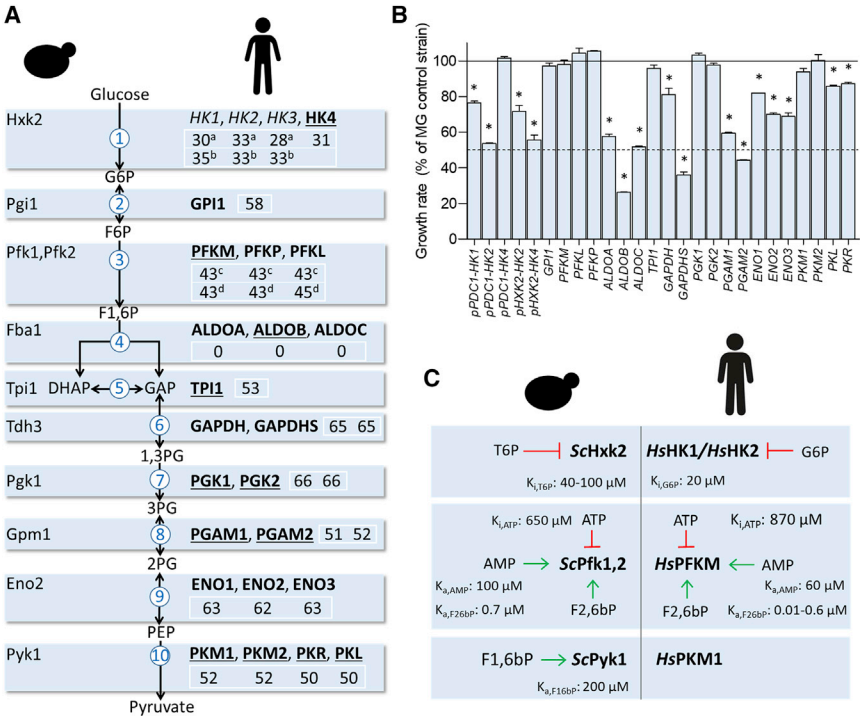

Figure 1. Glycolytic human and yeast enzymes relevant for this study and single complementation assays

(A) Major glycolytic isoenzymes in yeast (left) and human used in this study (right). Underlined human enzymes were known to complement their yeast ortholog. Bold enzymes complemented their yeast counterpart in this study. Percentage identity at the protein level is shown for the human enzymes compared with their yeast orthologs: a and b, first subunit and second subunit of human hexokinases versus *Sc*Hxk2, respectively; c and d, human phosphofructokinases versus *Sc*Pfk1 and *Sc*Pfk2, respectively. See also Table S1.

(B) Specific growth rates of the single gene complementation strains grown in SM glucose, shown as percentage of the MG control strain IMX372. See also Figure S1. *HsHK2* and *HsHK4* were expressed with the *ScPDC1* promoter or the *ScHXK2* promotor, leading to different growth rates. Shown is the average and standard deviation of at least three independent replicates. *p < 0.01 between the complementation and control strain (Student's t test, two-tailed, homoscedastic).

(C) Main allosteric regulators of the glycolytic yeast and human kinases and their regulation constants (Blazquez et al., 1993; Wilson, 2003; van Eunen et al., 2012; Lambeth and Kushmerick, 2002; Hohmann et al., 1996; Teusink et al., 2000).

1925). So far, few single human glycolytic enzymes have been transplanted into yeast, mostly in large-scale complementation studies (Hamza et al., 2020; Heinisch, 1993; Kachroo et al., 2015; Laurent et al., 2020; Lu et al., 2007a; Mayordomo and Sanz, 2001). Whether all human glycolytic enzymes can complement their yeast orthologs is still unknown. It is a particularly fascinating question because glycolytic enzymes, in yeast and human, are endowed with moonlighting capabilities (Sriram et al., 2005; Gancedo and Flores, 2008). The degree of conservation of moonlighting functions between these two distant organisms has hardly been explored to date, with the exception of human aldolase B (*Hs*ALDOB) and glucokinase (*Hs*HK4) (Lu et al., 2007a; Mayordomo and Sanz, 2001).

To overcome the difficulty caused by genetic redundancy, a yeast strain in which the set of genes encoding glycolytic enzymes has been minimized from 19 to 11 has been constructed previously (Solis-Escalante et al., 2015). This minimal glycolysis (MG) strain is a perfect platform for single glycolytic gene complementation. Furthermore, a strain in which this minimized set of yeast glycolytic genes has been fully relocated to a single chromosomal locus (SwYG strain) enables swapping of the entire yeast glycolytic pathway by any designer glycolysis with minimal genetic engineering (Kuijpers et al., 2016). In the present study, glycolysis swapping in the SwYG strain was used to evaluate the functionality of an entire human muscle glycolytic pathway in yeast. A combination of single gene complementation, full pathway humanization, and adaptive laboratory evolution was used to explore the functionality of all human glycolytic genes in yeast. This led to identification of mutations in human hexokinase 1 and 2, related to allosteric inhibition by glucose-6-phosphate, required for functional expression in yeast. Finally, the validity of yeast strains with humanized glycolysis as a model was evaluated by comparing the protein turnover number (k_{cat}) of the human glycolytic enzymes expressed in yeast and in human skeletal muscle myotube cell cultures.

RESULTS

All human glycolytic genes directly complement their yeast ortholog except for hexokinases 1–3

With the exception of hexokinases and F1,6bP aldolases, human and yeast glycolytic enzymes are highly conserved, with 43%–66% identity at the protein level compared with 32% identity at whole-proteome level (Kachroo et al., 2015; Figure 1A). The human and yeast F1,6bP-aldolases do not share homology at the protein level (Marsh and Lebherz, 1992; Figure 1A; Table S1). Among the four human hexokinases (*Hs*HK1–*Hs*HK4), *Hs*HK4 is closest in size and sequence to *Sc*Hxk2 (~30% protein identity), whereas *Hs*HK1–*Hs*HK3 are roughly twice the size of their yeast orthologs, each subunit sharing approximately 30% identity with *Sc*Hxk2 (Cárdenas et al., 1998; Table S1). Because of the genetic redundancy of metabolic pathways in eukaryotes (Steinke et al., 2006; Gordon et al., 2009), complementation in *S. cerevisiae* has so far only been tested for eight human glycolytic genes (Hamza et al., 2015; Heinisch, 1993; Kachroo et al., 2015; Laurent et al., 2020; Mayordomo and Sanz, 2001), of which only *HsPGAM2* was unsuccessful (Table S1; Laurent et al., 2019, 2020). Using the MG yeast strain, which carries a single isoenzyme for each glycolytic step (with the exception of the *Sc*Pfk1 and *Sc*Pfk2 subunits of the hetero-octameric phosphofructokinase; Solis-Escalante et al., 2015), 25 human glycolytic genes were tested for their ability to individually complement their yeast

A

Strain name	Exposed to glucose	Mutation in HK
Complementation strain *Hs*HK1		
IMX1689[a]	No	None
IMS1137[a]	Yes	Gly-679-Ala
IMS1140[a]	Yes	Gly-679-Ala
IMS1143[a]	Yes	Gly-896-Ala
Complementation strain *Hs*HK2		
IMX2419[a]	No	None
IMX1690[a]	Yes	Leu-776-Phe
IMX2419-M1[a]	Yes	Thr-457-Pro
IMX2419-M2[a]	Yes	Val-206-Del
IMX1873[b]	Yes	Thr-457-Ile
Fully humanized strain *Hs*HK2		
IMX2496[b]	No	None
IMX1844[b]	Yes	Ile-562-Asn
IMX2418[b]	Yes	Leu-126-Del
IMX2496-M1[b]	Yes	Asp-209-Asn

[a] expressed with *PDC1* promotor
[b] expressed with *HXK2* promotor

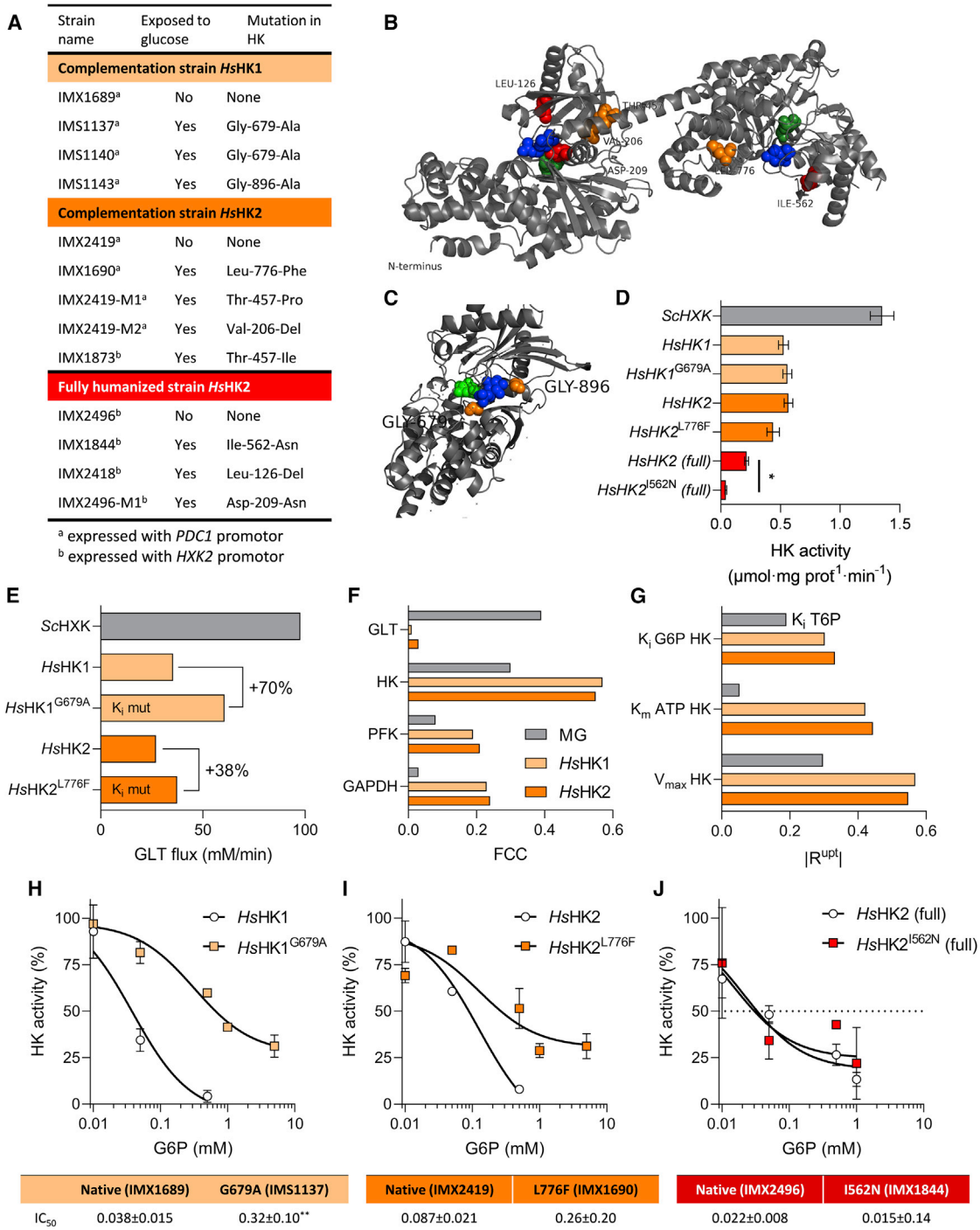

	Native (IMX1689)	G679A (IMS1137)	Native (IMX2419)	L776F (IMX1690)	Native (IMX2496)	I562N (IMX1844)
IC_{50}	0.038±0.015	0.32±0.10**	0.087±0.021	0.26±0.20	0.022±0.008	0.015±0.14

Figure 2. Characterization of human hexokinase mutants

(A) Mutations in human hexokinases after growth on glucose.

(B and C) Localization of the amino acid substitutions in *Hs*HK2 and *Hs*HK1 mutants, respectively. Color coding is as in (A). Green, glucose binding site in the catalytic domain; blue, G6P allosteric binding site. The *Hs*HK2 crystal structure is from Nawaz et al. (2018), and that of *Hs*HK1 is from Aleshin et al. (1998).

(D) Hexokinase *in vitro* activity from *S. cerevisiae* strains grown on SM galactose. *Sc*Hxk2 control activity was measured using strain IMX2015. Non-mutated *Hs*HK1 and *Hs*HK2 were assayed using strains IMX1689, IMX2419, and IMX2496 (*Hs*Gly-HK2), which were never exposed to glucose. Activities of the mutated variants were measured in extracts obtained from IMS1137, IMX1690, and IMX1844. In the complementation strains and the control *Sc*Hxk strain, hexokinase was expressed with the strong *ScPDC1* promoter, and in the fully humanized strains, the *ScHXK2* promotor was used. Shown are the average and standard deviation of biological duplicates. An asterisk indicates significant change in activity compared with native enzymes (*$p < 0.01$, $n = 2$, unpaired t test).

(legend continued on next page)

ortholog(s) (Figure 1A). For enzymes with multiple splicing variants, the canonical version was used (Figure 1A; Table S1), with the exception of pyruvate kinases *HsPKLR* and *HsPKM*, for which all four tissue-specific splicing variants were tested (Figure 1A; Table S1; Israelsen and Vander Heiden, 2015). The 25 genes were codon optimized and constitutively expressed as single copy in the MG strain, resulting in 25 humanized strains (Table S2; Figure S1A). Remarkably, 22 of these 25 human genes readily complemented their yeast orthologs for growth on glucose (Figures 1B and S1). *HsHK1* and *HsHK2,* but not *HsHK3*, were also complementary, but only after a period of adaptation of several days. Although most strains were marginally affected by humanization, strains harboring human hexokinase 2, aldolases, phosphoglycerate mutases, and the glyceraldehyde 3-phosphate dehydrogenase (GAPDH) variant S had a strongly reduced growth rate, with the strongest decrease (70%) occurring with *Hs*ALDOB (Figure 1B). No correlation was found between growth rate and conservation in human and yeast gene sequences or promoter strength (Figures S1C and S1D). All human genes besides *HsHK1* and *HsHK2* maintained their native sequence in yeast. This study therefore demonstrates the absence of complementation of the native human *HsHK3* and the remarkable complementation by 22 of 25 human genes of their yeast orthologs.

Human *Hs*HK1 and *Hs*HK2 can only complement the yeast hexokinases upon mutation

Upon transformation, strains expressing human *HsHK1* or *HsHK2* as the sole hexokinase grew well on galactose, a carbon source that does not require hexokinase activity, and displayed native *HsHK1* and *HsHK2* sequences. However exposure to glucose led to 1–2 days of lag phase and systematic occurrence of single mutations in *HsHK1* and *HsHK2*, causing amino acid substitution or deletion (Figures 2A–2C). *Hs*HK1 and *Hs*HK2 of strains solely exposed to galactose were active *in vitro* (strains IMX1689 and IMX2419, respectively), revealing that impaired growth on glucose was most likely not caused by lack of functionality of the human hexokinases in yeast (Figure 2D). Because native and mutated alleles of human hexokinases (strains IMS1137 and IMX1690) had similar catalytic activity *in vitro* (Figure 2D), growth defects on glucose might result from inhibition of native human hexokinases in yeast. The mutations might alleviate this inhibition to enable hexokinase activity *in vivo*. Mutations were observed in different regions of the *HsHK2* sequence in different strains, whereas, in three separate *HsHK1* mutants, the mutations were reproducibly localized at the glucose-6-phosphate (G6P) binding site (Figures 2B and 2C). The activity of both human hexokinases is sensitive to substrate concentration (Nawaz et al., 2018; Ardehali et al., 1996) but is also allosterically inhibited by the product of the reaction, G6P (Tsai and Wilson, 1996; Ardehali et al., 1996). The elevated intracellular G6P concentrations reported for yeast (0.5–2 mM) are well above the $K_{i,G6P}$ of *Hs*HK1 and *Hs*HK2 (0.02 mM) and might inhibit these enzymes in yeast (Wilson, 2003; Lagunas and Gancedo, 1983).

A computational "hexokinase complementation model" built to address this phenomenon predicted a functional glycolytic pathway able to reach a stable flux for *Hs*HK1 and *Hs*HK2 with glucose as a carbon source (Figure 2E) but with a remarkable shift in control of the glycolytic flux from glucose import (as predicted with yeast hexokinases) to hexokinase, as demonstrated by the increased flux control coefficient (FCC) (Figure 2F). The glycolytic flux was more specifically predicted to be sensitive to the magnitude of the $K_{i,G6P}$, $K_{m,ATP}$, and V_{max} of both hexokinases (Figure 2G). In agreement with this prediction, the tested hexokinase mutants of *Hs*HK1 and *Hs*HK2 (*Hs*HK1^{G679A} from IMS1137 and *Hs*HK2^{L776F}) were less sensitive to G6P inhibition than the native alleles (Figures 2H and 2I). These results are in contrast with a previous study, in which the *Hs*HK1^{G679A} mutation did not alter inhibition by the G6P analog 1,5-anhydroglucitol-6P of purified *Hs*HK1 expressed in *Escherichia coli* (Zeng et al., 1998). The $K_{i,G6P}$ of the humanized computational glycolytic model was modified using our experimental data (Figures 2H and 2I) to mimic the response of the mutated *Hs*HK1^{G679A} and *Hs*HK2^{L776F} variants, predicting an increase in glycolytic flux of 70% for *Hs*HK1^{G679A} and 38% for *Hs*HK2^{L776F} compared with their native variants (Figure 2E). Conversely, the sensitivity of the native and L776F variants to ATP, ADP, and glucose measured *in vitro* were similar (Figure S2), and trehalose-6-phosphate, a major inhibitor of yeast hexokinase not present in human cells, only mildly affected human hexokinase activity *in vitro* and the predicted *in silico* glycolytic flux (Figure S2; Blazquez et al., 1993). G6P inhibition is therefore most likely the main mechanism underlying the inability of native *Hs*HK1 and *Hs*HK2 to complement their yeast ortholog.

Successful humanization of the entire glycolytic pathway in yeast

Encouraged by the successful individual complementation, full pathway transplantation was attempted. Its success depends on expression, kinetic, and moonlighting properties of the whole set of enzymes (Figure 1C), which, combined, may severely affect the yeast host. The muscle glycolytic pathway, characterized by fast *in vivo* rates, was chosen for transplantation in yeast (Crowther et al., 2002a, 2002b; van Hall, 2010). Isoenzymes found to be most expressed in muscle tissue in public databases were selected. *Hs*HK1 and *Hs*HK2 are the most abundant hexokinase isoforms in muscle tissue (Grossbard and Schimke, 1966;

(E) Simulated glucose uptake rate (GLT, glucose transporter) for the MG control, native *Hs*HK1 and *Hs*HK2 complementation strains. The effect of the observed change in $K_{i,G6P}$ on the flux is modeled for each enzyme.
(F) Flux control coefficients (FCCs) of the four enzymes with the highest control over the flux, GLT, hexokinase (HK), phosphofructokinase (PFK) and glyceraldehyde 3-phosphate dehydrogenase (GAPDH).
(G) Absolute values of the response coefficient $|R^{upt}|$ of the three parameters with highest control over the steady-state glucose uptake flux.
(H–J) *In vitro* activity of the native and mutated HK variants at various concentrations of the competitive inhibitor G6P, expressed as percentage of activity without inhibitor. IC_{50}, half maximal inhibitory concentration of G6P (mM). Error bars represent standard deviation of duplicates. Asterisks indicate a significant difference of the mutated compared with the native variant (**$p < 0.01$, extra-sum-of-squares F test, $n = 2$).

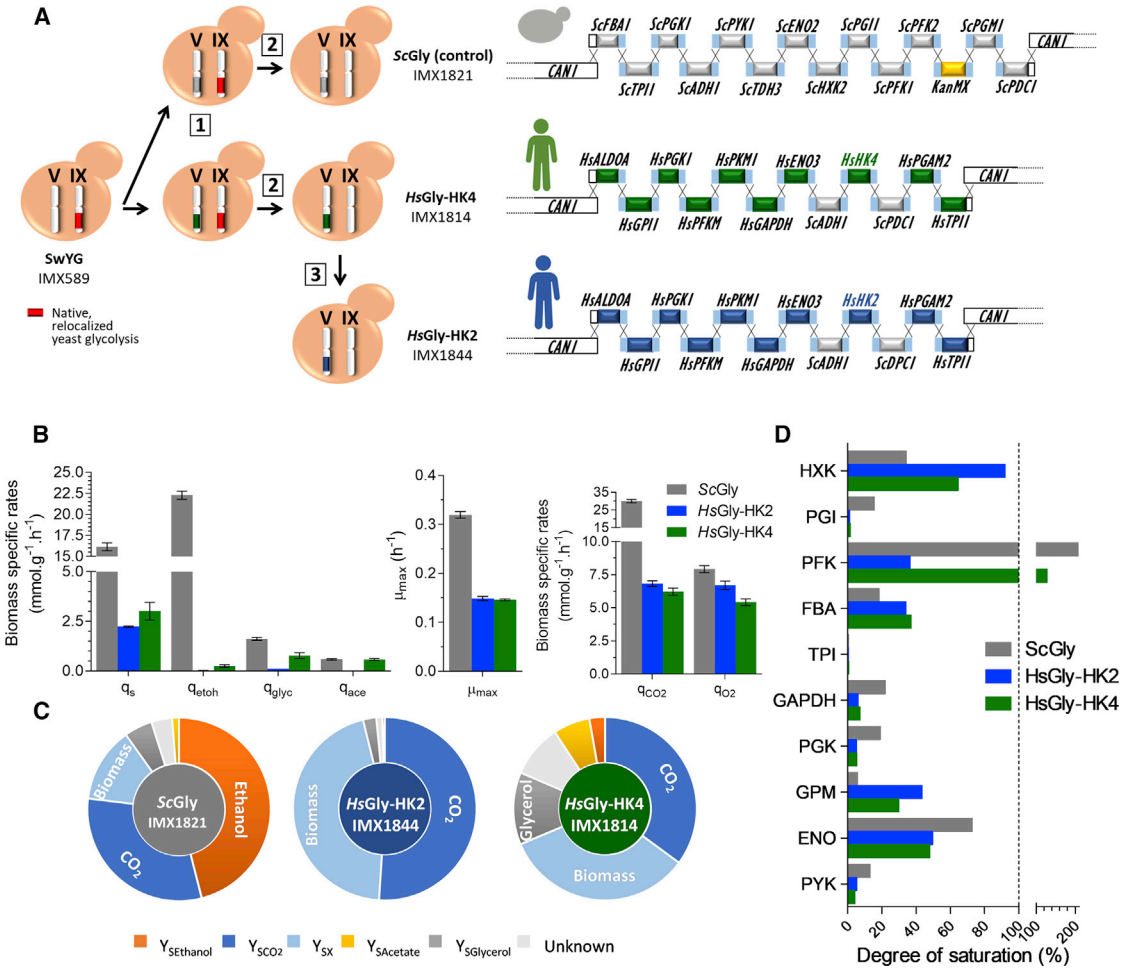

Figure 3. Construction and physiological characterization of strains with fully humanized glycolysis

(A) Construction strategy and glycolytic pathway in strains with native and humanized co-localized glycolysis.

(B–D) Physiological characterization of strains shown in (A) in duplicate bioreactors on SM glucose.

(B) Specific rates for glucose and oxygen uptake (q_S and q_{O2}) and for ethanol (qetOH), glycerol (q_{glyc}), acetate (q_{ace}), CO_2 (q_{CO2}), and biomass (μ_{max}) production. Shown are the average and SEM of biological duplicates. (C) Yields on glucose (CMol/CMol) of ethanol, CO_2, biomass, acetate, and glycerol are indicated ($Y_{SEthanol}$, Y_{SCo2}, Y_{SX}, $Y_{SAcetate}$, and $Y_{Sglycerol}$, respectively).

(D) Estimation of the degree of saturation of glycolytic enzymes based on *in vitro* assays from cell extracts (activities reported in Figure S6). *In vivo* fluxes were approximated from q_S. The dashed line indicates 100% saturation.

Ritov and Kelley, 2001), and *Hs*HK2, usually annotated as the main muscle isoenzyme, was chosen. *Hs*HK2 was also particularly interesting to assess if mutations found with single complementation were also required for functionality in a human glycolytic context. Although not the most abundant in muscle tissue, *Hs*HK4 was also chosen as hexokinase because of its ability to readily complement *Sc*Hxk2 and its sequence, kinetic, and regulatory differences from *Hs*HK2 (substantially lower affinity for glucose and insensitivity to G6P) (Bell et al., 1996; Matschinsky, 1990; Cárdenas et al., 1998). Transplantation in a SwYG strain (Kuijpers et al., 2016) of the entire set of human glycolytic genes resulted in the *Hs*Gly-HK2 strain with *Hs*HK2 and the *Hs*Gly-HK4 strain with *Hs*HK4 (Figure 3A; Table S2). Expression of *HsHK2* and *HsHK4* using the yeast *ScHXK2* promoter in these fully humanized strains led to a slower growth rate than complementation using the stronger *ScPDC1* promoter (Figures 1B and S1). Pathway transplantation was successful for the *Hs*Gly-HK2 and *Hs*Gly-HK4 strains (growth rate ~0.15 h^{-1}; around 40% of the control SwYG strain with native glycolysis *Sc*Gly [IMX1821]) in minimal medium with glucose as the sole carbon source (Figure 3B). As observed for the single complementation strain, growth on glucose of the *Hs*Gly-HK2 strain occurred after a long lag phase and required single mutations in the vicinity of the catalytic and G6P binding sites of *HsHK2* (Figure 2A; Table S3). An approximately 5-fold decrease in hexokinase V_{max} was observed in an isolate carrying the *Hs*Gly-HK2^{I562N} variant, but no other changes in kinetic parameters were observed (Figures 2D, 2J, and S3). In another isolate, the *Hs*HK2^{D209N} mutation affected a key amino acid of the C-terminal active site (Ardehali et al., 1996). The decrease in V_{max} but

maintenance of G6P sensitivity of *Hs*HK2^{I562N} was in stark contrast with the stable V_{max} but decreased G6P sensitivity observed for *Hs*HK2 variants in single complementation strains (Figures 2H–2J). This suggested differences in the intracellular environment of the fully humanized strains (particularly metabolite concentrations), leading to different requirements for hexokinase functionality and different evolutionary solutions.

Human and yeast pyruvate kinases also differ in allosteric regulations, with *Hs*PKM1 insensitive to feedforward activation by F1,6bP, characteristic of *Sc*Pyk1 (Figures 1C and S4). Despite the proposed role of this allosteric regulation for yeast cellular adaption to transitions (van Heerden et al., 2014; Boles et al., 1997), humanized yeast strains performed well during transition between an alternative (galactose) and favorite (glucose) carbon source (Figure S5).

S. cerevisiae favors a mixed respiro-fermentative metabolism when glucose is present in excess (see IMX1821 in Figures 3B and 3C), a phenomenon known as the Crabtree effect, analogous to the Warburg effect in mammalian cells (Diaz-Ruiz et al., 2009). *Hs*Gly-HK2 mostly respired glucose, with only traces of ethanol and glycerol being produced, whereas *Hs*Gly-HK4 displayed a respiro-fermentative metabolism more similar to that of the *Sc*Gly control strain but with far lower substrate uptake and ethanol production rates (Figures 3B and 3C; Table S4). The phenotypic similarity between fully humanized and *Hs*HK2 and *Hs*HK4 single complementation strains suggested that the human hexokinases strongly contributed to this switch between fermentative and respiratory metabolism but might not be the only players (Figure 4A). Except for *Hs*GPI1, the activity of the human enzymes was 2–50 times lower than the activity of their yeast ortholog (Figure S6). With the notable exception of phosphofructokinase, sensitive *in vivo* to many effectors, the yeast glycolytic enzymes generally operate at overcapacity (Van den Brink et al., 2008; Tai et al., 2007; Jansen et al., 2005; Figure 3D). In the humanized yeast strains, hexokinase, aldolase, and phosphoglycerate mutase showed higher degrees of saturation compared with the control strain with native yeast glycolysis, suggesting that the activity of these enzymes could exert higher control on glycolytic flux in the humanized strains (Figure 3D). Accordingly, these three enzymes also led to low growth rates in single complementation strains (Figure 1B). Remarkably, the activity of *Hs*PFKM was 2.6-fold lower in *Hs*Gly-HK4 than in *Hs*Gly-HK2, but the same protein abundance was found (Figure S6). Although *Hs*PFKM *in vivo* operated above its *in vitro* capacity in *Hs*Gly-HK4, similarly to what is typically observed in *S. cerevisiae* and in IMX1821, the flux through *Hs*PFKM in *Hs*Gly-HK2 was only at approximately 30% of its *in vitro* capacity (Figure 3D).

Overall, transplantation of a complete human glycolytic pathway to yeast was successful despite the structural, kinetic, and regulatory differences between yeast and human enzymes. Global proteomics revealed increases in the fully humanized strains of protein abundance of mainly metabolic enzymes (e.g., respiratory chain, TCA cycle), in line with the altered physiology (Figure S7). The fully humanized glycolysis strains grew remarkably well. The reduced glycolytic flux and growth rate, compared with yeast strains with native glycolysis (μ_{max} ~60% slower), matched the lower *in vitro* capacity of the human glycolytic enzymes.

Complementation of moonlighting functions

Many eukaryotic glycolytic enzymes have other "moonlighting" cellular activities in addition to their glycolytic function. Failure of the human orthologs to complement the yeast moonlighting functions could strongly affect the humanized yeast strains, but little is known about conservation of moonlighting functions across species (Gancedo and Flores, 2008). Three glycolytic enzymes in *S. cerevisiae* have documented moonlighting functions: hexokinase, aldolase, and enolase.

*Sc*Hxk2 is involved in glucose repression and the Crabtree effect by localizing to the nucleus and repressing a wide range of genes in the presence of excess glucose. *SUC2*, encoding invertase, is repressed with excess glucose and expressed and active in low-glucose medium (Figures 4A and 4B; Fernandez-Garcia et al., 2012; Herrero et al., 1998). Double *ScHXK1* and *ScHXK2* deletion enables invertase expression in the presence of excess glucose. Invertase assays suggested that *Hs*HK4, but not *Hs*HK2^{L776F}, was able to complement the role in glucose repression of *Sc*Hxk2 (Figures 4A and 4B). However, because invertase repression is known to be sensitive to growth rate and the *Hs*HK2-Gly strains grew slowly, our findings do not completely rule out the possibility that *Hs*HK2 plays a role in glucose repression, but, based on the difference in sequence, size, and structure with yeast hexokinase, this seems unlikely. The role of *Hs*HK4 in glucose repression, suggested in an earlier report (Mayordomo and Sanz, 2001), is in line with the Crabtree effect observed for complementation and fully humanized strains carrying *Hs*HK4 despite their slow growth rate (Figures 3B and 3C; Elbing et al., 2004; Van Hoek et al., 1998).

Yeast aldolase is involved in assembly of vacuolar proton-translocating ATPases (V-ATPases), a function required for growth at alkaline pH (Lu et al., 2004). This function is conserved between the yeast Fba1 and the human *Hs*ALDOB despite the absence of sequence homology between the two proteins (Lu et al., 2004, 2007b). In the present study, complementation by the other human aldolases, *Hs*ALDOA and *Hs*ALDOC, which share approximately 70% identity with *Hs*ALDOB, was also performed. All three human aldolase complementation strains as well as the fully humanized strains *Hs*Gly-HK2 and *Hs*Gly-HK4 showed no growth defects at pH 7.5 (Figures 4C and S8), indicating that the vacuolar function was complemented by all three human aldolases.

Yeast enolase plays a role in mitochondrial import of tRNA^{Lys}, a mechanism important for growth at temperatures above 37°C, particularly on non-fermentable carbon sources (Entelis et al., 2006; Schneider, 2011). This mechanism seems to be well conserved in mammals because yeast tRK1 is imported *in vitro* and *in vivo* in human mitochondria in an enolase-dependent manner (Entelis et al., 2001; Kolesnikova et al., 2004; Baleva et al., 2015). All three human enolase complementation strains show only minor growth defects at 37°C on glucose and non-fermentable carbon sources compared with the MG control strain (Figure 4D). The fully humanized strains also show no growth defect at 37°C (Figure S8). This suggests that the human enolase enzymes are also able to fully take over the mitochondrial import role of tRK1. The yeast enolases *Sc*Eno1 and *Sc*Eno2 are also involved in vacuolar fusion and protein transport to the vacuole (Decker and Wickner, 2006). Whether the human

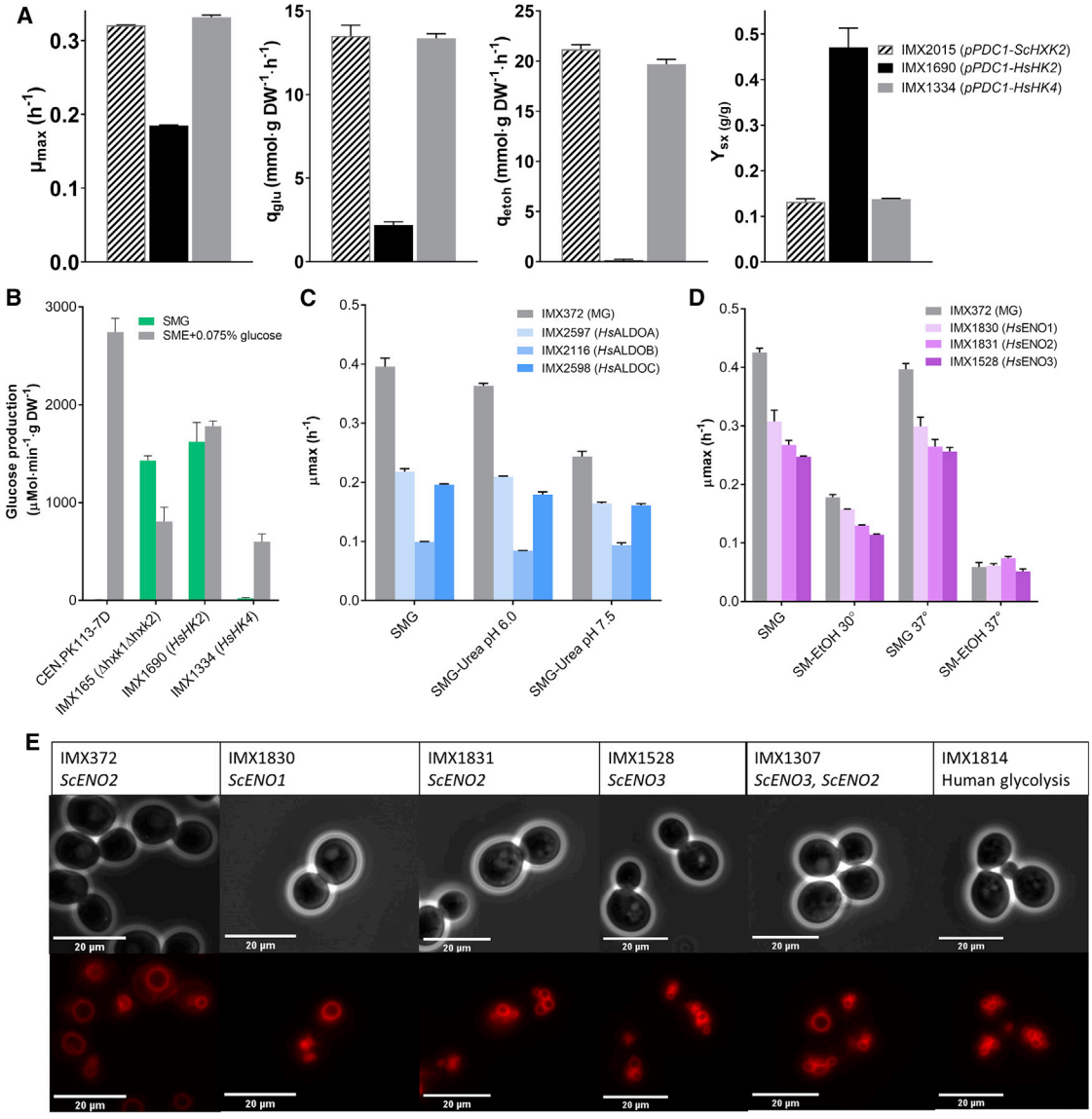

Figure 4. Complementation of moonlighting functions

(A) Specific growth (μ_{max}), glucose consumption (q_{glu}), and ethanol production (q_{etoh}) rates and biomass yield (Y_{SX}) of single HK complementation strains grown in a shake flask in SM glucose. Shown is the average and SEM of two biological replicates.

(B) Extracellular invertase activity of cultures with SM glucose (repressing condition) or SM ethanol +0.075% glucose (inducing condition). Shown are the average and SEM of two biological replicates.

(C and D) Specific growth rate of strains with single complementation of the three human aldolases and the three human enolases and of the MG control strain at different pH levels or at 30°C and 37°C, with glucose or ethanol as a carbon source, as indicated. Shown are the average and standard deviation of biological triplicates. SM medium was used, but ammonium was replaced with urea to maintain pH in (C).

(E) Staining of membranes with FM4-64 in *S. cerevisiae* strains expressing the yeast *Sc*Eno2 (IMX372 control) or the human *Hs*ENO1, *Hs*ENO2, and *Hs*ENO3 (IMX1830, IMX1831, and IMX1528, respectively) as single complementation or fully humanized glycolysis (*Hs*ENO 3 and IMX1814, respectively). IMX1307 carries one copy of the human *HsENO3* gene and the yeast *ScENO2* gene.

enolases can take over this function in yeast is unknown. Although enolase-deficient yeast strains display a fragmented vacuole phenotype and growth defects, this phenotype was not observed in the MG strain expressing *Sc*Eno2 only (Solis-Escalante et al., 2015; Figure 4E) and was also not observed for complementation strains expressing any of the three human enolases (Figure 4E). Therefore, this vacuolar moonlighting function seems to be conserved between yeast and human enolases.

With the exception of *Hs*HK2, no phenotypic defects previously associated with an absence of glycolytic moonlighting activities could be observed in the humanized strains, suggesting that, under the tested conditions, the moonlighting functions of

all glycolytic enzymes could be sufficiently complemented by their human orthologs.

Engineering and evolutionary approaches to accelerate the slow growth of humanized glycolysis strains

Several enzymes (*Hs*HK2, *Hs*HK4, *Hs*ALDOA, and *Hs*PGAM2) showed a significantly higher degree of saturation in the humanized strains (2- to 6-fold higher compared with *Sc*Gly; Figure 3D). The corresponding complementation strains also grew slower than the control strain, suggesting that the capacity of these enzymes might be limiting the glycolytic flux. Simultaneous overexpression of *HsHK2*, *HsALDOA*, and *HsPGAM2* in *Hs*Gly-HK2 and of *HsHK4*, *HsALDOA*, and *HsPGAM2* in *Hs*Gly-HK4 successfully increased their specific growth rate by 63% and 48%, respectively (Figure 5A). These optimized, humanized yeast strains still grew 30%–40% slower than the control strain with native, minimized yeast glycolysis (Figure 5A). Growth at 37°C, the optimal temperature for human enzymes, instead of 30°C did not improve the growth rate of the humanized yeast strains (Figures 5A and S8).

Many other mechanisms could explain the slow growth phenotype of the humanized strains, such as (allosteric) inhibition of the enzymes *in vivo*, incompatibility of substrate and cofactor concentrations with enzyme kinetic requirements, or deleterious effects of moonlighting activities of the human orthologs, more than could reasonably be tested by design-build-test-learn approaches. An adaptive laboratory evolution (ALE) strategy, particularly powerful to elucidate complex phenotypes (Sandberg et al., 2019), was therefore used to improve the fitness of the humanized strains. After approximately 630 generations in glucose medium, evolved populations of humanized yeast strains grew approximately 2-fold faster than their *Hs*Gly-HK2 and *Hs*Gly-HK4 ancestors (Figure S9). This increase in growth rate was confirmed in single-colony isolates from six independent evolution lines, three per humanized yeast strain (strains IMS0987–IMS0993; Figure 5A). These strains evolved toward higher glycolytic flux and a more fermentative metabolism, producing ethanol, but with a lower yield compared with the *Sc*Gly control (Figure S9). This increase in fermentation was in line with the increased specific growth rate and glucose uptake rate (Elbing et al., 2004). These evolved strains were further characterized in an attempt to elucidate the molecular basis of the humanized yeast strains slow growth phenotype.

Exploring the causes of the slow growth phenotype of humanized glycolysis strains

The activity of several human glycolytic enzymes was affected by evolution (Figure S10). Across the six evolution lines, the activity of both hexokinases (*Hs*HK2 and *Hs*HK4) and *Hs*PGAM2, for which activity was much lower than their yeast variants, was increased 2- to 3-fold during evolution (Figures 5B and 5C). These enzymes also led to the strongest decrease in growth rate upon single complementation (Figures 1B and S10). The protein abundance of *Hs*HK4 and *Hs*PGAM2 was increased accordingly, albeit not with the same magnitude, but the change in *in vitro* activity of *Hs*HK2 was not reflected in protein abundance (Figures 5C and S10). The activity of *Hs*ALDOA, which also led to a large decrease in growth rate upon complementation and for which the activity was strongly reduced in the fully humanized strains, was not markedly altered by evolution. The response of *Hs*PFKM was particularly interesting. Although its activity was already lower in the humanized yeast strains than in the *Sc*Gly strain, *Hs*PFKM was the only enzyme for which the activity was substantially decreased during evolution, by a factor of 2–8, compared with its non-evolved humanized ancestor. For *Hs*HK2 and *Hs*PFKM, the changes in *in vitro* activity were not reflected in protein abundance. Global proteomics showed that few proteins changed significantly in abundance during evolution (Figure S11).

With the exception of *Hs*PFKM, the genome sequence of the evolved strains offered little insight into the mechanisms leading directly to the abovementioned alterations in *in-vitro*-specific activities or abundance of glycolytic enzymes. However, interesting mutations were identified. The promoter, coding, and terminator regions of the human glycolytic genes were exempt from mutations in the evolved strains. Only *Hs*PFKM carried a single mutation in its coding region in all three evolution lines of *Hs*Gly-HK4 (Figure 5D; Table S5), one located in the N-terminal catalytic domain of the protein and two in the C-terminal regulatory domain, where several allosteric effectors can bind (F2,6biP, ATP, ADP, citrate, etc.; Sola-Penna et al., 2010; Banaszak et al., 2011). The effect of these mutations cannot be inferred directly from location, but they are most likely involved in the strong decrease in *in vitro* activity of *Hs*PFKM in the strains evolved from *Hs*Gly-HK4. All three *Hs*Gly-HK4 evolved strains also harbored an amino acid substitution in Tup1, a general transcriptional repressor involved in glucose repression (Figure 5D; Table S5). The glycolytic transcription factors (Rap1, Abf1, Gcr1, and Gcr2) were not mutated in any strain. Overall, few mutations were common across the evolved strains, with the exception of a single gene, *STT4*, for which mutations were found in all six evolution lines (Figure 5D). Remarkably, the six identified mutations were located within 164 amino acids, in the C terminus of the protein harboring the catalytic domain (Table S5). *STT4* encodes a phosphatidylinositol-4P (PI4P) kinase that catalyzes phosphorylation of PI4P into $PI4,5P_2$. Because Stt4 is essential in yeast (Trotter et al., 1998), the mutations in the evolved strains could not cause loss of function. Phosphoinositides are important signaling molecules in eukaryotes, involved in vacuole morphology and cytoskeleton organization via actin remodeling (Audhya et al., 2000). PI4P kinases are conserved eukaryotic proteins (Tolias and Cantley, 1999), and Stt4 shares similarities with human phosphatidylinositol 3-kinase (PI3K) (Yoshida et al., 1994). In mammals, activation of PI3K remodels actin, releasing aldolase A trapped in the actin cytoskeleton in an inactive state and increasing cellular aldolase activity (Hu et al., 2016; Kusakabe et al., 1997). Because yeast and human forms of actin are highly conserved (89% identity at the protein level), a similar mechanism could be active in yeast and enable the evolved, humanized yeast strains to increase aldolase activity *in vivo* without increasing its concentration. Reverse engineering of two of the mutations found in the evolved strains IMS0990 and IMS0992 was performed in the non-evolved strain backgrounds with native yeast glycolysis and humanized glycolysis by mutating the native *STT4* gene (Figure 5A). The increases in

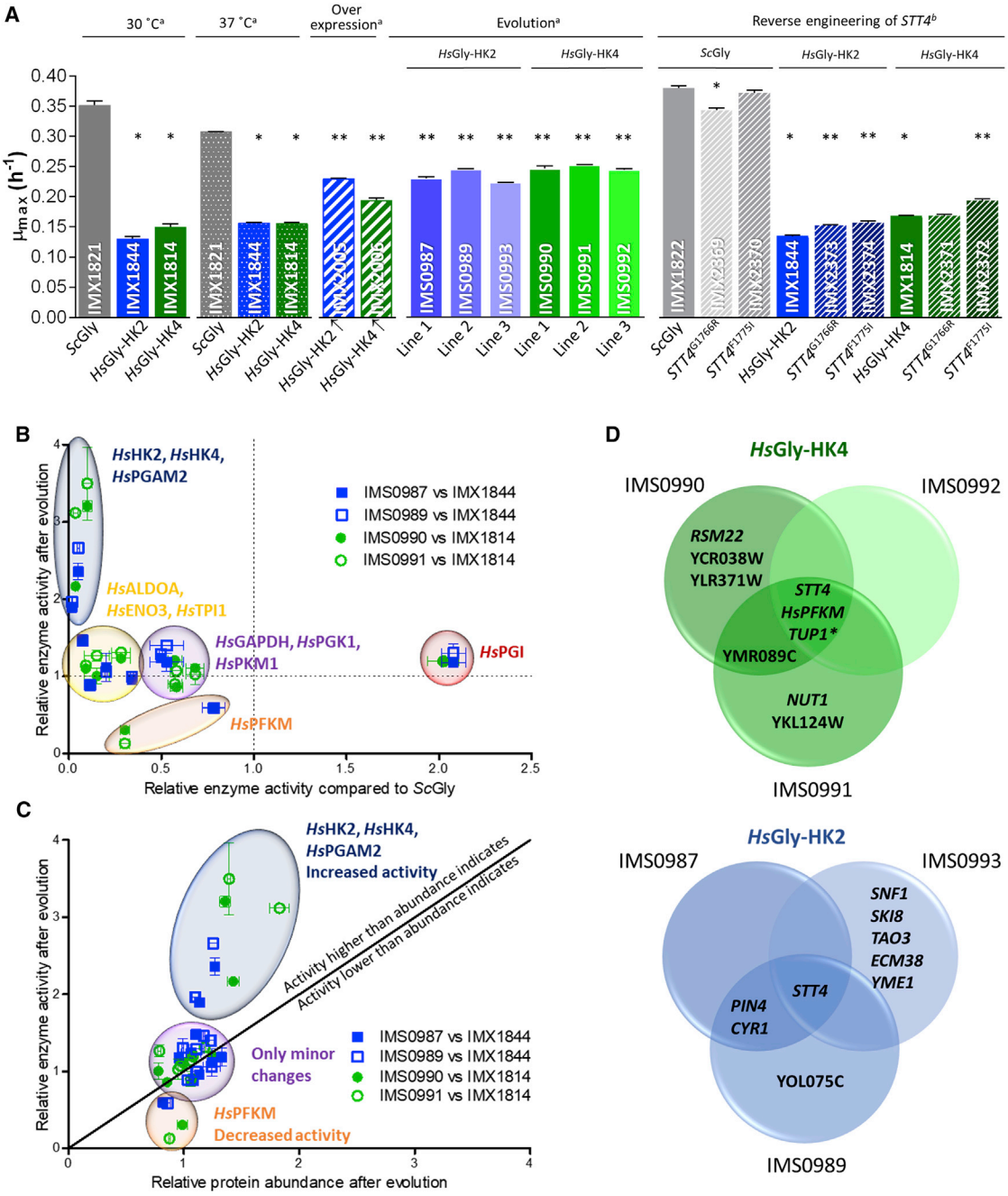

Figure 5. Strategies to improve the growth rates of fully humanized yeast strains

(A) Specific growth rate of humanized, evolved, and reverse-engineered strains in SM glucose; shown is the SEM of at least duplicates. One asterisk indicates significant differences between *Hs*Gly-HK2 or *Hs*Gly-HK4 and the control strain IMX1821 and two asterisks significant differences between the evolved and reverse-engineered strains and their respective parental strain *Hs*Gly-HK2 or *Hs*Gly-HK4 (n = 2, Student's t test, two tailed, homoscedastic; *,**$p < 0.05$). a, aerobic shake flasks; b, growth profiler.

(B) Comparison between the changes in glycolytic enzyme activity caused by humanization of yeast glycolysis and by evolution of the humanized strains. Activities can be found in Figures S6 and S10. Shown are the average and SEM of biological duplicates. Enzymes with a similar response are grouped.

(C) Comparison of changes in enzyme activity and in protein abundance caused by evolution of the humanized yeast strains. Error bars represent SEM of duplicate enzyme activity measurements and triplicate proteomics measurements.

(D) Mutations found in single-colony isolates from independent evolution lines of humanized yeast strains.

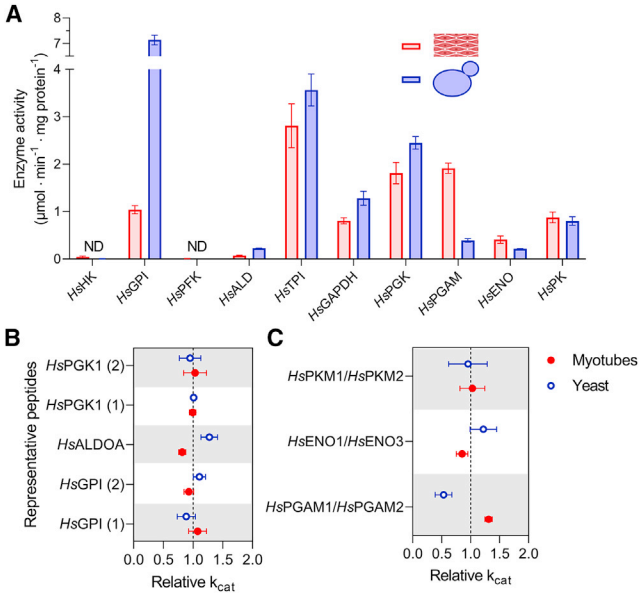

Figure 6. Enzyme activity and k_{cat} of human glycolytic enzymes in human myotubes and humanized yeast

(A) Specific activity of human glycolytic enzymes *in vitro* with *in-vivo*-like assay conditions. Blue, yeast strain *Hs*Gly-HK2; red, muscle myotube cultures.

(B and C) k_{cat} values for enzymes present as a single isoform (B) or multiple isoforms (C) in the myotube proteome data (Figure S13). Data represent the mean values and SEM of three and two independent culture replicates for the myotube and yeast cultures, respectively. ND, not detected.

specific growth rate did not match the growth rates of the evolved strains, suggesting other parallel mechanisms. Interestingly, in the reverse-engineered strains, *STT4* mutations resulted in a fragmented vacuole phenotype (Figure S12), confirming that the mutations interfered with Stt4 activity and PI4P signaling. Such a phenotype was not observed in the evolved strains, but, in these strains, vacuoles also displayed abnormal morphologies with collapsed structures, indicating that specific mechanisms might have evolved in parallel to mitigate the effect of *STT4* mutations on vacuolar morphology (Figure S12).

These findings suggest that evolution led to optimization of human glycolytic pathway function in yeast through several mechanisms. Hexokinase 4 and phosphoglycerate mutase abundance and activity increased, allowing higher glycolytic flux. For hexokinase 2 and phosphofructokinase, posttranslational mechanisms to modify enzyme activity must be present, counterintuitively decreasing *Hs*PFKM activity *in vitro*. In all evolution lines, mutations in Stt4 occurred, which could potentially benefit *in vivo* aldolase activity through modulation of actin structures. These adaptations reveal that the enzymes with the largest effect on growth rate in single complementation models (*Hs*HK2, *Hs*HK4, *Hs*PGAM2, and *Hs*ALDOA), and not those with the lowest activity, are the main targets for evolution. Changes in enzyme abundance, cellular environment, and posttranslational modifications, and not direct mutations of the glycolytic genes, appear to be the most effective evolutionary strategy to improve flux of this heterologous pathway.

Relevance of yeast as model for human glycolysis

To explore whether the yeast intracellular environment interfered with folding or posttranslational modifications of human enzymes, the catalytic rate constant (k_{cat}) of the human glycolytic proteins in yeast and in their native, human environment in myotubes was experimentally determined. Enzyme activities were measured in cell extracts using *in-vivo*-like assay conditions. In these assays, phosphofructokinase and hexokinase activities were too low for detection, although both could be detected at the protein level (Figure S13). Overall, the V_{max} of glycolytic enzymes was of the same order of magnitude in humanized yeast and muscle cells (Figure 6A). *Hs*GPI1, *Hs*ALDOA, *Hs*GAPDH, and *Hs*PGK1 activity was higher in yeast cells than in muscle cells, particularly for *Hs*GPI1 (7-fold), whereas the activity of *Hs*PGAM2 was 5.5-fold lower in yeast compared with muscle cells (Figure 6A). The differences in *in vitro* activity between yeast and human isoenzymes were mirrored in the peptide abundance of these proteins (Figure S13), suggesting that the turnover rates of the human proteins expressed in human and yeast cells were not substantially different.

The k_{cat} values of *Hs*GPI, *Hs*ALDOA, and *Hs*PGK1 revealed no differences between yeast and myotubes, irrespective of which of the standard peptides was used for protein quantification (Figures S13C and 6B). For the remaining enzymes, calculation of the turnover rate was complicated by the presence of isoenzymes other than the canonical muscle glycolytic enzymes in myotube cultures. In addition to the canonical muscle isoenzymes, the isoenzymes *Hs*PFKL, *Hs*PGAM1, and *Hs*ENO1 were present at equivalent or higher concentrations, and *Hs*HK1, *Hs*PFKP, and *Hs*PKM2 were present in low concentrations (Figure S13). This difference in isoenzyme abundance between tissue and isolated cell lines has been reported before for *in vitro* muscle cultures and, to a lower extent, for muscle biopsies (Deshmukh et al., 2015). Therefore, for enolase, phosphoglycerate mutase, and pyruvate kinase, the apparent k_{cat} was assumed to be the V_{max} divided by the sum of all detected isoforms catalyzing the specific reaction. The k_{cat} values of *Hs*ENO1 and *Hs*ENO3 have been reported to be similar (Shimizu et al., 1983), but *Hs*PGAM2 and *Hs*PKM1 have a higher k_{cat} than their respective isozymes (Durany et al., 1996; Harkins et al., 1977). Taking this into account, apparent k_{cat} values for enolase and pyruvate kinase were similar in humanized yeast and myotubes, whereas the k_{cat} of *Hs*PGAM was lower in humanized yeast (2.5-fold lower than in myotubes) (Figure 6C). This may suggest that the yeast intracellular environment has a negative effect on posttranslational processing of the enzyme or the influence of the *Hs*PGAM2 isozyme in muscle cells. These results demonstrate that, of the six enzymes for which a turnover rate could be determined, five were not catalytically altered by the yeast environment, with *Hs*PGAM2 as a potential exception.

DISCUSSION

The human glycolytic genes showed remarkable complementation in yeast, individually and as a complete pathway, with conservation of their secondary functions and turnover numbers similar to human muscle glycolysis. The combinations of strains presented here can thus serve as new models to study

fundamental aspects of human glycolysis in a simplified experimental setting, including moonlighting functions, the effects of post-translational modifications and allosteric regulators, and cross-talk between enzymes. The extensive tractability and genetic accessibility of yeast enables fast construction and testing of libraries of humanized yeast strains with different glycolytic designs.

The requirement of single amino acid substitutions in human hexokinases 1 and 2 for complementation in yeast illustrates that these enzymes have evolved to function in a particular metabolic niche. The ease of complementation with the human glycolytic genes is remarkable because glycolytic enzymes are known to be involved in numerous different moonlighting functions in yeast and human cells. In line with earlier work (Mayordomo and Sanz, 2001), we found that *Hs*HK4, but not *Hs*HK2, can complement the yeast Hxk2 for invertase repression. The ability of *Hs*HK4 to transduce glucose signaling in yeast is surprising because this enzyme has not been reported to regulate transcription in human cells. *Hs*HK4 also lacks the decapeptide required for translocation of *Sc*Hxk2 to the nucleus and its binding to the Mig1 transcription factor, although it has been shown previously to localize to the yeast nucleus (Herrero et al., 1998; Ahuatzi et al., 2004; Riera et al., 2008). The secondary function of yeast aldolase and enolase in vacuolar ATPase assembly, vacuolar fusion and transport, and mitochondrial tRNA import was complemented by all human aldolase and enolase isozymes. This extraordinary conservation of glycolytic moonlighting functions challenges our understanding of the underlying molecular mechanisms and reveals evolutionarily conserved functions.

The availability of a library of yeast strains with humanization of the entire glycolytic pathway and single complementation offers a unique opportunity to study potential synergetic effects between glycolytic enzymes and the effect of a full pathway on individual enzymes. A good example is the different evolutionary strategies of fully humanized and single complementation strains to restore functionality of human hexokinases. All single complementation strains alleviated G6P inhibition on *Hs*Hk1 and *Hs*Hk2, whereas a fully humanized strain reduced *Hs*Hk2 activity without altering G6P sensitivity. G6P is a key metabolite at the branchpoint of several pathways in yeast and human. Although the capacity for glycogen synthesis and hexokinase activity, as measured by their V_{max}, does not largely differ between yeast and skeletal muscle (Albe et al., 1990; Bogardus et al., 1984; Teusink et al., 2000; Gollnick et al., 1974; Simoneau and Bouchard, 1989), several differences between yeast and muscle could account for the higher cellular G6P levels found in yeast (Wilson, 2003; Lagunas and Gancedo, 1983). Regulation of glucose uptake is very different in yeast and muscle cells. In skeletal muscle, glycolytic fluxes are very dynamic and respond to physiological status (such as meal status and exercise), a response largely controlled by glucose transport (Hansen et al., 1995; Ren et al., 1993) and ATP demand (Schmitz et al., 2010). Even when at maximum capacity upon stimulation by insulin, glucose uptake is approximately two orders of magnitude lower than in yeast cells, and the muscle environment offers a much higher phosphorylation/uptake ratio than yeast. Other differences influencing G6P concentration could be the presence of the trehalose cycle (Argüelles, 2014) and the greater capacity of G6P dehydrogenase, the first step of the pentose phosphate pathway, in yeast as compared with human muscle (Albe et al., 1990; Heinisch et al., 2020; Bresolin et al., 1989; Battistuzzi et al., 1985). G6P plays a role in modulating gene expression in human cells via the ChREBP and MondoA-MIX transcription factor complexes (Li et al., 2010; Peterson et al., 2010). These factors contribute to differences in cellular G6P levels between yeast and skeletal cells, resulting in supra-inhibitory levels of *Hs*HK1 and *Hs*HK2 in the yeast context. The different evolutionary strategy found in strains with fully humanized glycolysis might originate from different factors. Isomerization of G6P into F6P does most likely not account for large differences in G6P levels in fully humanized and single complementation strains because human *Hs*PGI and native *Sc*Pgi1 operate near equilibrium and have similar *in vitro* activity (Canelas et al., 2011). Conversely, the substantially lower activity of several human glycolytic enzymes compared with their yeast equivalent (e.g., ALDOA and PGAM activities are ~10-fold lower) and resulting low glycolytic flux might alter metabolite concentrations in yeast and, therefore, the selection pressure exerted on hexokinase. Measuring cellular metabolite concentrations should shed some light on the effect of partial and full humanization on the yeast cellular context. Another difference between human and yeast hexokinase 2 is the VDAC-dependent mitochondrial binding in human, which is not likely to be conserved in the humanized strains unless the human VDAC protein is heterologously expressed (Blachly-Dyson et al., 1993; Wilson, 1997). Humanization of glucose transport or mitochondrial VDAC proteins in yeast could elucidate specific aspects of human hexokinases regulation and function in a human-like context.

A potential crosstalk between *Hs*PFKM and hexokinase was also revealed by comparing single gene and full pathway transplantation. *Hs*PFKM displayed 2.5-fold higher *in vitro* activity in a strain expressing *Hs*HK2 as the sole hexokinase compared with a strain expressing *Hs*HK4, whereas protein abundance was identical. In the *Hs*Gly-HK4 strain, the low *in vitro* activity of *Hs*PFKM activity did not match the predicted *in vivo* activity based on observed fluxes. This discrepancy between *in vitro* and *in vivo* was even stronger in evolved isolates of *Hs*Gly-HK4, in which *Hs*PFKM was systematically mutated. Conversely, no mutations were found in *Hs*PFKM in the evolved *Hs*Gly-HK2 strains. *Hs*PFKM is regulated at multiple levels (e.g., post-translational modification, binding to the cytoskeleton, etc.) and most likely does not operate optimally in yeast (Sola-Penna et al., 2010; Raïs et al., 2000). Stabilization of *Hs*PFKM oligomerization promoted by calmodulin in human cells might be impaired in yeast, considering the difference between yeast and human calmodulin (~60% identity at the protein level) (Marinho-Carvalho et al., 2009; Schmitz et al., 2013). The present results suggest the existence of a still unknown hexokinase-dependent mechanism controlling *Hs*PFKM.

ALE and overexpression identified hexokinase and *Hs*PGAM2 as critical enzymes for glycolytic flux and growth rate improvement of the fully humanized strains. *Hs*PGAM2's lower activity and k_{cat} compared with human myotube cells suggested that the yeast environment is unfavourable for this enzyme, a problem that both humanized strains solved by increasing *Hs*PGAM2

activity. The suboptimal activity of the hexokinases was solved similarly during evolution. However, for *Hs*PGAM2 and *Hs*HK2 as well as *Hs*PFKM, which decreased in activity during evolution, the changes in *in vitro* activity in evolved strains could not be fully explained by the changes in protein abundance and did not result from mutations in non-coding or coding regions of the corresponding genes. Modulation of enzyme activity through interactions with the cellular environment or direct posttranslational covalent modifications are most likely responsible for this discrepancy between protein level and *in vitro* enzyme activity. Several human glycolytic proteins are regulated via interaction with the cytoskeleton. In mammals, aldolase interacts with actin, whose remodeling is signaled via phosphoinositide and PI3K. The systematic mutation in the evolved humanized strains of *STT4*, encoding a PI4-kinase involved in cellular signaling for many cellular processes, including actin organization in yeast, suggests that ALDOA activity might also be modulated in yeast by binding to actin and altered by phosphoinositide-mediated signaling. Overall optimization of human glycolysis in yeast seems to be largely exerted by posttranslational mechanisms, and ALE is a powerful strategy to identify mechanisms causing suboptimal functionality in yeast.

This first successful humanization of skeletal muscle glycolysis in yeast offers new possibilities to explore human glycolysis. Because many complex interactions with various organelles and signaling pathways that are present in human cells are absent in yeast, such model strains can be applied to study the pathway in a "clean" background. Transplantation to the yeast context enables dissection of metabolic from signaling-related mechanisms in control and regulation of glucose metabolism, mechanisms often debated in the field of diabetes and muscle insulin resistance. As an example, whether glycolytic enzymes themselves could be inhibited by intermediates of lipid metabolism in muscle and consequently affect enzyme activity and glycolytic fluxes remains an open question to be tested (Jenkins et al., 2011; Thompson and Cooney, 2000). Beyond muscle tissue, the glycolysis swapping concept can be extended to any glycolytic configuration. Complete pathway transplantation can be used in the future to generate translational microbial models to study fundamental aspects of evolutionary conservation between species and tissues and unravel mechanisms of related diseases.

Limitations of this study

Although this work demonstrates that pathway swapping enables fast and facile transplantation of an entire pathway, a general limitation of the proposed approach is the characterization of the physiological and cellular effect of the transplantation. Comprehensively capturing all effects of such drastic genetic changes is very time and resource consuming, which has guided the decision for the present manuscript to focus on a subset of human glycolytic isoenzymes for humanization and on in-depth characterization of a few important findings, such as hexokinases. Many of the intriguing results uncovered by this study could not (yet) lead to mechanistic understanding and require further research. Although ALE did bring new insight into the interaction between human glycolytic isoenzymes and the yeast environment, many questions remain unanswered, such as the mechanisms that cause the reduction in growth rate in humanized strains or those that enable yeast cells to tune the abundance of human glycolytic proteins. Finally, an unfortunate technical limitation prevented measurement of human hexokinase and phosphofructokinase activity in yeast and human cells using *in-vivo*-like assay conditions. The reasons for this lack of *in vitro* activity have to be further explored to complete the comparison of glycolytic human enzyme functionality in yeast and human contexts.

STAR★METHODS

Detailed methods are provided in the online version of this paper and include the following:

- KEY RESOURCES TABLE
- RESOURCE AVAILABILITY
  - Lead contact
  - Materials availability
  - Data and code availability
- EXPERIMENTAL MODEL AND SUBJECT DETAILS
  - Yeast and *E. coli* strains
  - Human myotube culture
- METHOD DETAILS
  - Growth rate determinations and laboratory evolution
  - Molecular techniques, gene synthesis and Golden Gate plasmid construction
  - Construction of individual gene complementation strains
  - Full human glycolysis strain construction
  - *STT4* reverse engineering
  - Visualization of hexokinase mutants
  - Computational modeling of human hexokinase complementation
  - Construction of *Δhxk1Δhxk2* strain IMX165 and control strain IMX2015
  - Illumina whole genome sequencing
  - Quantitative aerobic batch cultivations
  - Sample preparation and enzymatic assays for comparison of yeast and humanized yeast samples
  - Invertase enzyme assay
  - Staining of vacuoles
  - Ploidy determination by flow cytometry
  - Transition experiment
  - Whole cell lysate proteomics of humanized yeast strains
  - Comparison human and humanized yeast glycolytic enzymes
- QUANTIFICATION AND STATISTICAL ANALYSIS

SUPPLEMENTAL INFORMATION

Supplemental information can be found online at https://doi.org/10.1016/j.celrep.2022.111010.

ACKNOWLEDGMENTS

We thank Jordi Geelhoed for reverse engineering and growth characterization, Agnes Hol and Ingeborg van Lakwijk for valuable work on the human hexokinase strains, and Lycka Kamoen, Eveline Vreeburg, and Daniel Solis-

Escalante for contributions to construction of reference strains. We thank Carol de Ram for processing proteomics samples, Pilar de la Torre and Marcel van den Broek for whole-genome sequencing and analysis, and Philip de Groot for help with bioreactors. This project was funded by the AdLibYeast European Research Council consolidator 648141 grant (to P.D.-L.), a UMCG-GSMS PhD fellowship, and the De Cock-Hadders Foundation.

AUTHOR CONTRIBUTIONS

F.J.B., E.K., and M.A.V.-L. designed and performed research and wrote the article. M.W. performed molecular biology and strain construction. M.A.H.L. performed enzyme activity and ploidy assays. K.v.E. set up *in-vivo*-like enzyme assays. M.d.R., J.C.W., and M.P. performed proteomics analyses. R.B. and A.M.A.S. set up and performed human myotube cultures. M.C.H. and P.v.R. provided material and input on *in silico* model development. J.M.D., B.B., and P.D.-L. designed and supervised the research and wrote the article.

DECLARATION OF INTERESTS

The authors declare no competing interests.

Received: October 22, 2021
Revised: February 3, 2022
Accepted: June 7, 2022
Published: June 28, 2022

REFERENCES

Agmon, N., Temple, J., Tang, Z., Schraink, T., Baron, M., Chen, J., Mita, P., Martin, J.A., Tu, B.P., Yanai, I., et al. (2020). Phylogenetic debugging of a complete human biosynthetic pathway transplanted into yeast. Nucleic Acids Res. *48*, 486–499. https://doi.org/10.1093/nar/gkz1098.

Ahuatzi, D., Herrero, P., De La Cera, T., and Moreno, F. (2004). The glucose-regulated nuclear localization of hexokinase 2 in *Saccharomyces cerevisiae* is Mig1-dependent. J. Biol. Chem. *279*, 14440–14446. https://doi.org/10.1074/jbc.m313431200.

Albe, K.R., Butler, M.H., and Wright, B.E. (1990). Cellular concentrations of enzymes and their substrates. J. Theor. Biol. *143*, 163–195. https://doi.org/10.1016/s0022-5193(05)80266-8.

Aleshin, A.E., Zeng, C., Bourenkov, G.P., Bartunik, H.D., Fromm, H.J., and Honzatko, R.B. (1998). The mechanism of regulation of hexokinase: new insights from the crystal structure of recombinant human brain hexokinase complexed with glucose and glucose-6-phosphate. Structure *6*, 39–50. https://doi.org/10.1016/s0969-2126(98)00006-9.

Almonacid Suarez, A.M., Zhou, Q., Van Rijn, P., and Harmsen, M.C. (2019). Directional topography gradients drive optimum alignment and differentiation of human myoblasts. J. Tissue. Eng. Regen. Med. *13*, 2234–2245. https://doi.org/10.1002/term.2976.

Ardehali, H., Yano, Y., Printz, R.L., Koch, S., Whitesell, R.R., May, J.M., and Granner, D.K. (1996). Functional organization of mammalian hexokinase II. J. Biol. Chem. *271*, 1849–1852. https://doi.org/10.1074/jbc.271.4.1849.

Argüelles, J.C. (2014). Why can't vertebrates synthesize trehalose? J. Mol. Evol. *79*, 111–116. https://doi.org/10.1007/s00239-014-9645-9.

Audhya, A., Foti, M., and Emr, S.D. (2000). Distinct roles for the yeast phosphatidylinositol 4-kinases, Stt4p and Pik1p, in secretion, cell growth, and organelle membrane dynamics. Mol. Biol. Cell *11*, 2673–2689. https://doi.org/10.1091/mbc.11.8.2673.

Baleva, M., Gowher, A., Kamenski, P., Tarassov, I., Entelis, N., and Masquida, B. (2015). A moonlighting human protein is involved in mitochondrial import of tRNA. Int. J. Mol. Sci. *16*, 9354–9367. https://doi.org/10.3390/ijms16059354.

Banaszak, K., Mechin, I., Obmolova, G., Oldham, M., Chang, S.H., Ruiz, T., Radermacher, M., Kopperschläger, G., and Rypniewski, W. (2011). The crystal structures of eukaryotic phosphofructokinases from baker's yeast and rabbit skeletal muscle. J. Mol. Biol. *407*, 284–297. https://doi.org/10.1016/j.jmb.2011.01.019.

Bárány, M. (1996). Biochemistry of Smooth Muscle Contraction (Elsevier).

Battistuzzi, G., D'urso, M., Toniolo, D., Persico, G.M., and Luzzatto, L. (1985). Tissue-specific levels of human glucose-6-phosphate dehydrogenase correlate with methylation of specific sites at the 3' end of the gene. Proc. Natl. Acad. Sci. U S A *82*, 1465–1469. https://doi.org/10.1073/pnas.82.5.1465.

Bell, G.I., Pilkis, S.J., Weber, I.T., and Polonsky, K.S. (1996). Glucokinase mutations, insulin secretion, and diabetes mellitus. Annu. Rev. Physiol. *58*, 171–186. https://doi.org/10.1146/annurev.ph.58.030196.001131.

Bertani, G. (1951). Studies on lysogenis I.: the mode of phage liberation by lysogenic *Escherichia coli*. J. Bacteriol. *62*, 293–300. https://doi.org/10.1128/jb.62.3.293-300.1951.

Bertani, G. (2004). Lysogeny at mid-twentieth century: P1, P2, and other experimental systems. J. Bacteriol. *186*, 595–600. https://doi.org/10.1128/jb.186.3.595-600.2004.

Blachly-Dyson, E., Zambronicz, E., Yu, W.H., Adams, V., Mccabe, E., Adelman, J., Colombini, M., and Forte, M. (1993). Cloning and functional expression in yeast of two human isoforms of the outer mitochondrial membrane channel, the voltage-dependent anion channel. J. Biol. Chem. *268*, 1835–1841. https://doi.org/10.1016/s0021-9258(18)53930-2.

Blázquez, M.A., Lagunas, R., Gancedo, C., and Gancedo, J.M. (1993). Trehalose-6-phosphate, a new regulator of yeast glycolysis that inhibits hexokinases. FEBS Lett. *329*, 51–54. https://doi.org/10.1016/0014-5793(93)80191-v.

Bogardus, C., Lillioja, S., Stone, K., and Mott, D. (1984). Correlation between muscle glycogen synthase activity and *in vivo* insulin action in man. J. Clin. Investig. *73*, 1185–1190. https://doi.org/10.1172/jci111304.

Boles, E., Schulte, F., Miosga, T., Freidel, K., SchlütEr, E., Zimmermann, F.K., Hollenberg, C.P., and Heinisch, J.J. (1997). Characterization of a glucose-repressed pyruvate kinase (Pyk2p) in *Saccharomyces cerevisiae* that is catalytically insensitive to fructose-1, 6-bisphosphate. J. Bacteriol. *179*, 2987–2993. https://doi.org/10.1128/jb.179.9.2987-2993.1997.

Boonekamp, F.J., Dashko, S., Van Den Broek, M., Gehrmann, T., Daran, J.M., and Daran-Lapujade, P. (2018). The genetic makeup and expression of the glycolytic and fermentative pathways are highly conserved within the *Saccharomyces* genus. Front. Genet. *9*, 504. https://doi.org/10.3389/fgene.2018.00504.

Breitwieser, G.E., Altamirano, A.A., and Russell, J.M. (1990). Osmotic stimulation of Na (+)-K (+)-Cl-cotransport in squid giant axon is [Cl-] i dependent. Am. J. Physiol. Cell Physiol. *258*, C749–C753. https://doi.org/10.1152/ajpcell.1990.258.4.c749.

Bresolin, N., Bet, L., Moggio, M., Meola, G., Fortunato, F., Comi, G., Adobbati, L., Geremia, L., Pittalis, S., and Scarlato, G. (1989). Muscle glucose-6-phosphate dehydrogenase deficiency. J. Neurol. *236*, 193–198. https://doi.org/10.1007/bf00314498.

Bruch, P., Schnackerz, K.D., and Gracy, R.W. (1976). Matrix-bound phosphoglucose isomerase: formation and properties of monomers and hybrids. Eur. J. Biochem. *68*, 153–158. https://doi.org/10.1111/j.1432-1033.1976.tb10773.x.

Canelas, A.B., Ras, C., Ten Pierick, A., Van Gulik, W.M., and Heijnen, J.J. (2011). An in vivo data-driven framework for classification and quantification of enzyme kinetics and determination of apparent thermodynamic data. Metab. Eng. *13*, 294–306. https://doi.org/10.1016/j.ymben.2011.02.005.

Cárdenas, M.L., Cornish-Bowden, A., and Ureta, T. (1998). Evolution and regulatory role of the hexokinases. Biochim. Biophys. Acta *1401*, 242–264. https://doi.org/10.1016/s0167-4889(97)00150-x.

Civelek, V.N., Hamilton, J.A., Tornheim, K., Kelly, K.L., and Corkey, B.E. (1996). Intracellular pH in adipocytes: effects of free fatty acid diffusion across the plasma membrane, lipolytic agonists, and insulin. Proc. Natl. Acad. Sci. U S A *93*, 10139–10144. https://doi.org/10.1073/pnas.93.19.10139.

Conley, K.E., Blei, M.L., Richards, T.L., Kushmerick, M., and Jubrias, S.A. (1997). Activation of glycolysis in human muscle *in vivo*. Am. J. Physiol. Cell Physiol. *273*, C306–C315. https://doi.org/10.1152/ajpcell.1997.273.1.c306.

Crowther, G.J., Carey, M.F., Kemper, W.F., and Conley, K.E. (2002a). Control of glycolysis in contracting skeletal muscle. I. Turning it on. Am. J. Physiol.

Endocrinol. Metab. *282*, E67–E73. https://doi.org/10.1152/ajpendo.2002.282.1.e67.

Crowther, G.J., Kemper, W.F., Carey, M.F., and Conley, K.E. (2002b). Control of glycolysis in contracting skeletal muscle. II. Turning it off. Am. J. Physiol. Endocrinol. Metab. *282*, E74–E79. https://doi.org/10.1152/ajpendo.2002.282.1.e74.

Cruz, A.L.B., Hebly, M., Duong, G.H., Wahl, S.A., Pronk, J.T., Heijnen, J.J., Daran-Lapujade, P., and Van Gulik, W.M. (2012). Similar temperature dependencies of glycolytic enzymes: an evolutionary adaptation to temperature dynamics? BMC Syst. Biol. *6*, 151. https://doi.org/10.1186/1752-0509-6-151.

Decker, B.L., and Wickner, W.T. (2006). Enolase activates homotypic vacuole fusion and protein transport to the vacuole in yeast. J. Biol. Chem. *281*, 14523–14528. https://doi.org/10.1074/jbc.m600911200.

Deshmukh, A.S., Murgia, M., Nagaraj, N., Treebak, J.T., Cox, J., Mann, M.J.M., and Proteomics, C. (2015). Deep proteomics of mouse skeletal muscle enables quantitation of protein isoforms, metabolic pathways, and transcription factors. Mol. Cell. Proteomics *14*, 841–853. https://doi.org/10.1074/mcp.m114.044222.

Diaz-Ruiz, R., Uribe-Carvajal, S., Devin, A., and Rigoulet, M. (2009). Tumor cell energy metabolism and its common features with yeast metabolism. Biochim. Biophys. Acta *1796*, 252–265. https://doi.org/10.1016/j.bbcan.2009.07.003.

Durany, N., Carreras, J., Biochemistry, P.P.B., and Biology, M. (1996). Distribution of phosphoglycerate mutase isozymes in rat, rabbit and human tissues, rabbit and human tissues. Comp. Biochem. Physiol. B Biochem. Mol. Biol. *114*, 217–223. https://doi.org/10.1016/0305-0491(95)02135-3.

Elbing, K., Larsson, C., Bill, R.M., Albers, E., Snoep, J.L., Boles, E., Hohmann, S., and Gustafsson, L. (2004). Role of hexose transport in control of glycolytic flux in *Saccharomyces cerevisiae*. Appl. Environ. Microbiol. *70*, 5323–5330. https://doi.org/10.1128/aem.70.9.5323-5330.2004.

Entelis, N., Brandina, I., Kamenski, P., Krasheninnikov, I.A., Martin, R.P., and Tarassov, I. (2006). A glycolytic enzyme, enolase, is recruited as a cofactor of tRNA targeting toward mitochondria in *Saccharomyces cerevisiae*. Genes Dev. *20*, 1609–1620. https://doi.org/10.1101/gad.385706.

Entelis, N.S., Kolesnikova, O.A., Martin, R.P., and Tarassov, I.A. (2001). RNA delivery into mitochondria. Adv. Drug. Deliv. Rev. *49*, 199–215. https://doi.org/10.1016/s0169-409x(01)00135-1.

Entian, K.-D., and Kötter, P. (2007). 25 Yeast genetic strain and plasmid collections. Methods Microbiol. *36*, 629–666. https://doi.org/10.1016/s0580-9517(06)36025-4.

Fell, D.A. (1992). Metabolic control analysis: a survey of its theoretical and experimental development. Biochem. J. *286* (*Pt 2*), 313–330.

Fernández-García, P., Peláez, R., Herrero, P., and Moreno, F. (2012). Phosphorylation of yeast hexokinase 2 regulates its nucleocytoplasmic shuttling. J. Biol. Chem. *287*, 42151–42164. https://doi.org/10.1074/jbc.m112.401679.

Flamholz, A., Noor, E., Bar-Even, A., and Milo, R. (2012). eQuilibrator—the biochemical thermodynamics calculator. Nucleic Acids Res. *40*, D770–D775. https://doi.org/10.1093/nar/gkr874.

Gancedo, C., and Flores, C.L. (2008). Moonlighting proteins in yeasts. Microbiol. Mol. Biol. Rev. *72*, 197–210, table of contents. https://doi.org/10.1128/mmbr.00036-07.

Garge, R.K., Laurent, J.M., Kachroo, A.H., and Marcotte, E.M. (2020). Systematic humanization of the yeast cytoskeleton discerns functionally replaceable from divergent human genes. Genetics *215*, 1153–1169. https://doi.org/10.1534/genetics.120.303378.

Gietz, R.D., and Woods, R.A. (2002). Transformation of yeast by lithium acetate/single-stranded carrier DNA/polyethylene glycol method. Methods Enzymol. *350*, 87–96. https://doi.org/10.1016/s0076-6879(02)50957-5.

Gollnick, P.D., Sjödin, B., Karlsson, J., Jansson, E., and Saltin, B. (1974). Human soleus muscle: a comparison of fiber composition and enzyme activities with other leg muscles. Pflügers Archiv *348*, 247–255. https://doi.org/10.1007/bf00587415.

Gordon, J.L., Byrne, K.P., and Wolfe, K.H. (2009). Additions, losses, and rearrangements on the evolutionary route from a reconstructed ancestor to the modern *Saccharomyces cerevisiae* genome. PLoS Genet. *5*, e1000485. https://doi.org/10.1371/journal.pgen.1000485.

Groen, A.K., Vervoorn, R.C., Van Der Meer, R., and Tager, J.M. (1983). Control of gluconeogenesis in rat liver cells. I. Kinetics of the individual enzymes and the effect of glucagon. J. Biol. Chem. *258*, 14346–14353. https://doi.org/10.1016/s0021-9258(17)43867-1.

Grossbard, L., and Schimke, R.T. (1966). Multiple Hexokinases of Rat Tissues: purification and comparison of soluble forms. J. Biol. Chem. *241*, 3546–3560. https://doi.org/10.1016/s0021-9258(18)99866-2.

Güldener, U., Heck, S., Fiedler, T., Beinhauer, J., Hegemann, J.H., and GUldener, U. (1996). A new efficient gene disruption cassette for repeated use in budding yeast. Nucleic Acids Res. *24*, 2519–2524. https://doi.org/10.1093/nar/24.13.2519.

Guynn, R.W., Veloso, D., Lawson, J.W.R., and Veech, R.L. (1974). The concentration and control of cytoplasmic free inorganic pyrophosphate in rat liver *in vivo*. Biochem. J. *140*, 369–375. https://doi.org/10.1042/bj1400369.

Haase, S.B., and Reed, S.I. (2002). Improved flow cytometric analysis of the budding yeast cell cycle. Cell Cycle *1*, 117–121. https://doi.org/10.4161/cc.1.2.114.

Hamilton, S.R., and Zha, D. (2015). Progress in yeast glycosylation engineering. Methods Mol. Biol. *1321*, 73–90. https://doi.org/10.1007/978-1-4939-2760-9_6.

Hamza, A., Driessen, M.R.M., Tammpere, E., O'neil, N.J., and Hieter, P. (2020). Cross-species complementation of nonessential yeast genes establishes platforms for testing inhibitors of human proteins. Genetics *214*, 735–747. https://doi.org/10.1534/genetics.119.302971.

Hamza, A., Tammpere, E., Kofoed, M., Keong, C., Chiang, J., Giaever, G., Nislow, C., and Hieter, P. (2015). Complementation of yeast genes with human genes as an experimental platform for functional testing of human genetic variants. Genetics *201*, 1263–1274. https://doi.org/10.1534/genetics.115.181099.

Hansen, P.A., Gulve, E.A., Marshall, B.A., Gao, J., Pessin, J.E., Holloszy, J.O., and Mueckler, M. (1995). Skeletal muscle glucose transport and metabolism are enhanced in transgenic mice overexpressing the Glut4 glucose transporter. J. Biol. Chem. *270*, 1679–1684. https://doi.org/10.1074/jbc.270.5.1679.

Harkins, R.N., Black, J.A., and Rittenberg, M.B. (1977). M2 isozyme of pyruvate kinase from human kidney as the product of a separate gene: its purification and characterization. Biochemistry *16*, 3831–3837. https://doi.org/10.1021/bi00636a018.

Heinisch, J.J. (1993). Expression of heterologous phosphofructokinase genes in yeast. FEBS Lett. *328*, 35–40. https://doi.org/10.1016/0014-5793(93)80960-3.

Heinisch, J.J., Knuesting, J., and Scheibe, R. (2020). Investigation of heterologously expressed glucose-6-phosphate dehydrogenase genes in a yeast *zwf1* deletion. Microorganisms *8*, 546. https://doi.org/10.3390/microorganisms8040546.

Herrero, P., Martínez-Campa, C., and Moreno, F. (1998). The hexokinase 2 protein participates in regulatory DNA-protein complexes necessary for glucose repression of the *SUC2* gene in *Saccharomyces cerevisiae*. FEBS Lett. *434*, 71–76. https://doi.org/10.1016/s0014-5793(98)00872-2.

Hohmann, S., Bell, W., NevesA, M.J., Valckx, D., and Thevelein, J.M. (1996). Evidence for trehalose-6-phosphate-dependent and-independent mechanisms in the control of sugar influx into yeast glycolysis. Mol. Microbiol. *20*, 981–991. https://doi.org/10.1111/j.1365-2958.1996.tb02539.x.

Hoops, S., Sahle, S., Gauges, R., Lee, C., Pahle, J., Simus, N., Singhal, M., Xu, L., Mendes, P., and Kummer, U. (2006). COPASI—a complex pathway simulator. Bioinformatics *22*, 3067–3074. https://doi.org/10.1093/bioinformatics/btl485.

Hu, H., Juvekar, A., Lyssiotis, C.A., Lien, E.C., Albeck, J.G., Oh, D., Varma, G., Hung, Y.P., Ullas, S., Lauring, J., et al. (2016). Phosphoinositide 3-kinase regulates glycolysis through mobilization of aldolase from the actin cytoskeleton. Cell *164*, 433–446. https://doi.org/10.1016/j.cell.2015.12.042.

Ingwall, J.S. (1982). Phosphorus nuclear magnetic resonance spectroscopy of cardiac and skeletal muscles. Am. J. Physiol. Heart. Circ. Physiol. *242*, H729–H744. https://doi.org/10.1152/ajpheart.1982.242.5.h729.

Ishibashi, H., and Cottam, G.L. (1978). Glucagon-stimulated phosphorylation of pyruvate kinase in hepatocytes. J. Biol. Chem. *253*, 8767–8771. https://doi.org/10.1016/s0021-9258(17)34243-6.

Israelsen, W.J., and Vander Heiden, M.G. (2015). Pyruvate kinase: function, regulation and role in cancer. Semin. Cell. Dev. Biol. *43*, 43–51. https://doi.org/10.1016/j.semcdb.2015.08.004.

Jansen, M.L.A., Diderich, J.A., Mashego, M., Hassane, A., De Winde, J.H., Daran-Lapujade, P., and Pronk, J.T. (2005). Prolonged selection in aerobic, glucose-limited chemostat cultures of *Saccharomyces cerevisiae* causes a partial loss of glycolytic capacity. Microbiology (Read.) *151*, 1657–1669. https://doi.org/10.1099/mic.0.27577-0.

Janssen, L.J., and Sims, S.M. (1992). Acetylcholine activates non-selective cation and chloride conductances in canine and Guinea-pig tracheal myocytes. J. Physiol. *453*, 197–218. https://doi.org/10.1113/jphysiol.1992.sp019224.

Jenkins, C.M., Yang, J., Sims, H.F., and Gross, R.W. (2011). Reversible high affinity inhibition of phosphofructokinase-1 by acyl-CoA: a mechanism integrating glycolytic flux with lipid metabolism. J. Biol. Chem. *286*, 11937–11950. https://doi.org/10.1074/jbc.m110.203661.

Kachroo, A.H., Laurent, J.M., Akhmetov, A., Szilagyi-Jones, M., Mcwhite, C.D., Zhao, A., and Marcotte, E.M. (2017). Systematic bacterialization of yeast genes identifies a near-universally swappable pathway. Elife *6*, e25093. https://doi.org/10.7554/elife.25093.

Kachroo, A.H., Laurent, J.M., Yellman, C.M., Meyer, A.G., Wilke, C.O., and Marcotte, E.M. (2015). Systematic humanization of yeast genes reveals conserved functions and genetic modularity. Science *348*, 921–925. https://doi.org/10.1126/science.aaa0769.

Kolesnikova, O.A., Entelis, N.S., Jacquin-Becker, C., Goltzene, F., Chrzanowska-Lightowlers, Z.M., Lightowlers, R.N., Martin, R.P., and Tarassov, I. (2004). Nuclear DNA-encoded tRNAs targeted into mitochondria can rescue a mitochondrial DNA mutation associated with the MERRF syndrome in cultured human cells. Hum. Mol. Genet. *13*, 2519–2534. https://doi.org/10.1093/hmg/ddh267.

Koning, M., Werker, P.M., Van Luyn, M.J., Krenning, G., and Harmsen, M.C. (2012). A global downregulation of microRNAs occurs in human quiescent satellite cells during myogenesis. Differentiation *84*, 314–321. https://doi.org/10.1016/j.diff.2012.08.002.

Kristensen, L.O. (1986). Associations between transports of alanine and cations across cell membrane in rat hepatocytes. Am. J. Physiol. Gastrointest. Liver. Physiol. *251*, G575–G584. https://doi.org/10.1152/ajpgi.1986.251.5.g575.

Kuijpers, N.G.A., Solis-Escalante, D., Luttik, M.A.H., Bisschops, M.M.M., Boonekamp, F.J., Van Den Broek, M., Pronk, J.T., Daran, J.M., and Daran-Lapujade, P. (2016). Pathway swapping: toward modular engineering of essential cellular processes. Proc. Natl. Acad. Sci. U S A *113*, 15060–15065. https://doi.org/10.1073/pnas.1606701113.

Kusakabe, T., Motoki, K., and Hori, K. (1997). Mode of interactions of human aldolase isozymes with cytoskeletons. Arch. Biochem. Biophys. *344*, 184–193. https://doi.org/10.1006/abbi.1997.0204.

Labunskyy, V.M., Suzuki, Y., Hanly, T.J., Murao, A., Roth, F.P., and Gladyshev, V.N. (2014). The insertion Green Monster (iGM) method for expression of multiple exogenous genes in yeast. G3 (Bethesda) *4*, 1183–1191. https://doi.org/10.1534/g3.114.010868.

Lagunas, R., and Gancedo, C. (1983). Role of phosphate in the regulation of the Pasteur effect in *Saccharomyces cerevisiae*. Eur. J. Biochem. *137*, 479–483. https://doi.org/10.1111/j.1432-1033.1983.tb07851.x.

Lambeth, M.J., and Kushmerick, M.J. (2002). A computational model for glycogenolysis in skeletal muscle. Ann. Biomed. Eng. *30*, 808–827. https://doi.org/10.1114/1.1492813.

Laurent, J.M., Garge, R.K., Teufel, A.I., Wilke, C.O., Kachroo, A.H., and Marcotte, E.M. (2019). Humanization of yeast genes with multiple human orthologs reveals principles of functional divergence between paralogs. Preprint at BioRxiv. https://doi.org/10.1101/668335.

Laurent, J.M., Garge, R.K., Teufel, A.I., Wilke, C.O., Kachroo, A.H., and Marcotte, E.M. (2020). Humanization of yeast genes with multiple human orthologs reveals functional divergence between paralogs. PLoS Biol. *18*, e3000627. https://doi.org/10.1371/journal.pbio.3000627.

Laurent, J.M., Young, J.H., Kachroo, A.H., and Marcotte, E.M. (2016). Efforts to make and apply humanized yeast. Briefings Funct. Genomics *15*, 155–163. https://doi.org/10.1093/bfgp/elv041.

Lee, M.E., Deloache, W.C., Cervantes, B., and Dueber, J.E. (2015). A highly characterized yeast toolkit for modular, multipart assembly. ACS Synth. Biol. *4*, 975–986. https://doi.org/10.1021/sb500366v.

Li, H., Handsaker, B., Wysoker, A., Fennell, T., Ruan, J., Homer, N., Marth, G., Abecasis, G., and Durbin, R. (2009). The sequence alignment/map format and SAMtools. Bioinformatics *25*, 2078–2079. https://doi.org/10.1093/bioinformatics/btp352.

Li, M.V., Chen, W., Harmancey, R.N., Nuotio-Antar, A.M., Imamura, M., Saha, P., Taegtmeyer, H., Chan, L.J.B., and Communications, B.R. (2010). Glucose-6-phosphate mediates activation of the carbohydrate responsive binding protein (ChREBP). Biochem. Biophys. Res. Commun. *395*, 395–400. https://doi.org/10.1016/j.bbrc.2010.04.028.

Lidofsky, S.D., Xie, M.-H., Sostman, A., Scharschmidt, B.F., and Fitz, J.G. (1993). Vasopressin increases cytosolic sodium concentration in hepatocytes and activates calcium influx through cation-selective channels. J. Biol. Chem. *268*, 14632–14636. https://doi.org/10.1016/s0021-9258(18)82380-8.

Lowry, O.H., Rosebrough, N.J., Farr, A.L., and Randall, R.J. (1951). Protein measurement with the Folin phenol reagent. J. Biol. Chem. *193*, 265–275. https://doi.org/10.1016/s0021-9258(19)52451-6.

Lu, M., Ammar, D., Ives, H., Albrecht, F., and Gluck, S.L. (2007a). Physical interaction between aldolase and vacuolar H+-ATPase is essential for the assembly and activity of the proton pump. J. Biol. Chem. *282*, 24495–24503. https://doi.org/10.1074/jbc.m702598200.

Lu, M., Ammar, D., Ives, H., Albrecht, F., and Gluck, S.L. (2007b). Physical interaction between aldolase and vacuolar H+-ATPase is essential for the assembly and activity of the proton pump. J. Biol. Chem. *282*, 24495–24503. https://doi.org/10.1074/jbc.m702598200.

Lu, M., Sautin, Y.Y., Holliday, L.S., and Gluck, S.L. (2004). The glycolytic enzyme aldolase mediates assembly, expression, and activity of vacuolar H+-ATPase. J. Biol. Chem. *279*, 8732–8739. https://doi.org/10.1074/jbc.m303871200.

Mans, R., Van Rossum, H.M., Wijsman, M., Backx, A., Kuijpers, N.G.A., Van Den Broek, M., Daran-Lapujade, P., Pronk, J.T., van Maris, A.J.A., and Daran, J.M.G. (2015). CRISPR/Cas9: a molecular Swiss army knife for simultaneous introduction of multiple genetic modifications in *Saccharomyces cerevisiae*. FEMS Yeast Res. *15*, fov004. https://doi.org/10.1093/femsyr/fov004.

Marinho-Carvalho, M.M., Costa-Mattos, P.V., Spitz, G.A., Zancan, P., and Sola-Penna, M. (2009). Calmodulin upregulates skeletal muscle 6-phosphofructo-1-kinase reversing the inhibitory effects of allosteric modulators. Biochim. Biophys. Acta *1794*, 1175–1180. https://doi.org/10.1016/j.bbapap.2009.02.006.

Marsh, J.J., and Lebherz, H.G. (1992). Fructose-bisphosphate aldolases: an evolutionary history. Trends Biochem. Sci. *17*, 110–113. https://doi.org/10.1016/0968-0004(92)90247-7.

Matschinsky, F.M. (1990). Glucokinase as glucose sensor and metabolic signal generator in pancreatic beta-cells and hepatocytes. Diabetes *39*, 647–652. https://doi.org/10.2337/diabetes.39.6.647.

Mayordomo, I., and Sanz, P. (2001). Human pancreatic glucokinase (GlkB) complements the glucose signalling defect of *Saccharomyces cerevisiae hxk2* mutants. Yeast *18*, 1309–1316. https://doi.org/10.1002/yea.780.

Mikkelsen, M.D., Buron, L.D., Salomonsen, B., Olsen, C.E., Hansen, B.G., Mortensen, U.H., and Halkier, B.A. (2012). Microbial production of

indolylglucosinolate through engineering of a multi-gene pathway in a versatile yeast expression platform. Metab. Eng. *14*, 104–111. https://doi.org/10.1016/j.ymben.2012.01.006.

Murphy, E., Steenbergen, C., Levy, L.A., Raju, B., and London, R.E. (1989). Cytosolic free magnesium levels in ischemic rat heart. J. Biol. Chem. *264*, 5622–5627. https://doi.org/10.1016/s0021-9258(18)83593-1.

Nawaz, M.H., Ferreira, J.C., Nedyalkova, L., Zhu, H., Carrasco-López, C., Carrasco-Lopez, C., Kirmizialtin, S., and Rabeh, W.M. (2018). The catalytic inactivation of the N-half of human hexokinase 2 and structural and biochemical characterization of its mitochondrial conformation. Biosci. Rep. *38*, BSR20171666. https://doi.org/10.1042/bsr20171666.

Nijkamp, J.F., Van Den Broek, M.A., Geertman, J.M.A., Reinders, M.J.T., Daran, J.M.G., and De Ridder, D. (2012). *De novo* detection of copy number variation by co-assembly. Bioinformatics *28*, 3195–3202. https://doi.org/10.1093/bioinformatics/bts601.

Nurse, P.M. (2002). Nobel lecture: cyclin dependent kinases and cell cycle control. Biosci. Rep. *22*, 487–499. https://doi.org/10.1023/a:1022017701871.

Oudard, S., Arvelo, F., Miccoli, L., Apiou, F., Dutrillaux, A., Poisson, M., Dutrillaux, B., and Poupon, M. (1996). High glycolysis in gliomas despite low hexokinase transcription and activity correlated to chromosome 10 loss. Br. J. Cancer. *74*, 839–845. https://doi.org/10.1038/bjc.1996.446.

Peterson, C.W., Stoltzman, C.A., Sighinolfi, M.P., Han, K.-S., Ayer, D.E., and Biology, C. (2010). Glucose controls nuclear accumulation, promoter binding, and transcriptional activity of the MondoA-Mlx heterodimer. Mol. Cell. Biol. *30*, 2887–2895. https://doi.org/10.1128/mcb.01613-09.

Petranovic, D., and Nielsen, J. (2008). Can yeast systems biology contribute to the understanding of human disease? Trends Biotechnol. *26*, 584–590. https://doi.org/10.1016/j.tibtech.2008.07.008.

Postma, E., Verduyn, C., Scheffers, W.A., and Van Dijken, J.P. (1989). Enzymic analysis of the crabtree effect in glucose-limited chemostat cultures of *Saccharomyces cerevisiae*. Appl. Environ. Microbiol. *55*, 468–477. https://doi.org/10.1128/aem.55.2.468-477.1989.

Prince, V.E., and Pickett, F.B. (2002). Splitting pairs: the diverging fates of duplicated genes. Nat. Rev. Genet. *3*, 827–837. https://doi.org/10.1038/nrg928.

Raïs, B., Ortega, F., Puigjaner, J., Comin, B., Orosz, F., Ovádi, J., Cascante, M., and Enzymology, M. (2000). Quantitative characterization of homo-and heteroassociations of muscle phosphofructokinase with aldolase. Biochim. Biophys. Acta *1479*, 303–314.

Ren, J.M., Marshall, B.A., Gulve, E.A., Gao, J., Johnson, D.W., Holloszy, J.O., and Mueckler, M. (1993). Evidence from transgenic mice that glucose transport is rate-limiting for glycogen deposition and glycolysis in skeletal muscle. J. Biol. Chem. *268*, 16113–16115. https://doi.org/10.1016/s0021-9258(19)85395-4.

Riera, A., Ahuatzi, D., Herrero, P., Garcia-Gimeno, M.A., Sanz, P., and Moreno, F. (2008). Human pancreatic β-cell glucokinase: subcellular localization and glucose repression signalling function in the yeast cell. Biochem. J. *415*, 233–239. https://doi.org/10.1042/bj20080797.

Rijksen, G., and Staal, G.E. (1977). Regulation of human erythrocyte hexokinase: the influence of glycolytic intermediates and inorganic phosphate. Biochim. Biophys. Acta *485*, 75–86. https://doi.org/10.1016/0005-2744(77)90194-2.

Ritov, V.B., and Kelley, D.E. (2001). Hexokinase isozyme distribution in human skeletal muscle. Diabetes *50*, 1253–1262. https://doi.org/10.2337/diabetes.50.6.1253.

Rorsman, P., and Trube, G. (1985). Glucose dependent K+-channels in pancreaticβ-cells are regulated by intracellular ATP. Pflügers Archiv *405*, 305–309. https://doi.org/10.1007/bf00595682.

Salazar, A.N., Gorter De Vries, A.R., Van Den Broek, M., Wijsman, M., De La Torre Cortes, P., Brickwedde, A., Brouwers, N., Daran, J.G., and Abeel, T. (2017). Nanopore sequencing enables near-complete de novo assembly of *Saccharomyces cerevisiae* reference strain CEN.PK113-7D. FEMS Yeast. Res. *17*, fox074.

Sandberg, T.E., Salazar, M.J., Weng, L.L., Palsson, B.O., and Feist, A.M. (2019). The emergence of adaptive laboratory evolution as an efficient tool for biological discovery and industrial biotechnology. Metab. Eng. *56*, 1–16. https://doi.org/10.1016/j.ymben.2019.08.004.

Santos, B., and Snyder, M. (2000). Sbe2p and sbe22p, two homologous Golgi proteins involved in yeast cell wall formation. Mol. Biol. Cell *11*, 435–452. https://doi.org/10.1091/mbc.11.2.435.

Schmitz, J.P.J., Groenendaal, W., Wessels, B., Wiseman, R.W., Hilbers, P.A.J., Nicolay, K., Prompers, J.J., Jeneson, J.A.L., and van Riel, N.A.W. (2013). Combined *in vivo* and *in silico* investigations of activation of glycolysis in contracting skeletal muscle. Am. J. Physiol. Cell Physiol. *304*, C180–C193. https://doi.org/10.1152/ajpcell.00101.2012.

Schmitz, J.P.J., Van Riel, N.A.W., Nicolay, K., Hilbers, P.A., Jeneson, J.A.L., and Jeneson, J.A. (2010). Silencing of glycolysis in muscle: experimental observation and numerical analysis. Exp. Physiol. *95*, 380–397. https://doi.org/10.1113/expphysiol.2009.049841.

Schneider, A. (2011). Mitochondrial tRNA import and its consequences for mitochondrial translation. Annu. Rev. Biochem. *80*, 1033–1053. https://doi.org/10.1146/annurev-biochem-060109-092838.

Shimizu, A., Suzuki, F., Kato, K., and Enzymology, M. (1983). Characterization of αα, ββ, γγ and αγ human enolase isozymes, and preparation of hybrid enolases (αγ, βγ and αβ) from homodimeric forms. Biochim. Biophys. Acta *748*, 278–284. https://doi.org/10.1016/0167-4838(83)90305-9.

Silveira, M.C., Carvajal, E., and Bon, E.P. (1996). Assay for *in vivo* yeast invertase activity using NaF. Anal. Biochem. *238*, 26–28. https://doi.org/10.1006/abio.1996.0244.

Simoneau, J.A., and Bouchard, C. (1989). Human variation in skeletal muscle fiber-type proportion and enzyme activities. Am. J. Phys. *257*, E567–E572. https://doi.org/10.1152/ajpendo.1989.257.4.e567.

Sola-Penna, M., Da Silva, D., Coelho, W.S., Marinho-Carvalho, M.M., and Zancan, P. (2010). Regulation of mammalian muscle type 6-phosphofructo-1-kinase and its implication for the control of the metabolism. IUBMB Life *62*, 791–796. https://doi.org/10.1002/iub.393.

Solis-Escalante, D., Kuijpers, N.G.A., Barrajon-Simancas, N., Van Den Broek, M., Pronk, J.T., Daran, J.M., and Daran-Lapujade, P. (2015). A minimal set of glycolytic genes reveals strong redundancies in *Saccharomyces cerevisiae* central metabolism. Eukaryot. Cell *14*, 804–816. https://doi.org/10.1128/ec.00064-15.

Solis-Escalante, D., Kuijpers, N.G., Bongaerts, N., Bolat, I., Bosman, L., Pronk, J.T., Daran, J.M., and Daran-Lapujade, P. (2013). *amdSYM*, a new dominant recyclable marker cassette for *Saccharomyces cerevisiae*. FEMS Yeast Res. *13*, 126–139. https://doi.org/10.1111/1567-1364.12024.

Sriram, G., Martinez, J.A., Mccabe, E.R., Liao, J.C., and Dipple, K.M. (2005). Single-gene disorders: what role could moonlighting enzymes play? Am. J. Hum. Genet. *76*, 911–924. https://doi.org/10.1086/430799.

Steinke, D., Hoegg, S., Brinkmann, H., and Meyer, A. (2006). Three rounds (1R/2R/3R) of genome duplications and the evolution of the glycolytic pathway in vertebrates. BMC Biol. *4*, 16. https://doi.org/10.1186/1741-7007-4-16.

Sun, S., Yang, F., Tan, G., Costanzo, M., Oughtred, R., Hirschman, J., Theesfeld, C.L., Bansal, P., Sahni, N., Yi, S., et al. (2016). An extended set of yeast-based functional assays accurately identifies human disease mutations. Genome Res. *26*, 670–680. https://doi.org/10.1101/gr.192526.115.

Tai, S.L., Daran-Lapujade, P., Luttik, M.a.H., Walsh, M.C., Diderich, J.A., Krijger, G.C., Van Gulik, W.M., Pronk, J.T., and Daran, J.M. (2007). Control of the glycolytic flux in *Saccharomyces cerevisiae* grown at low temperature - a multi-level analysis in anaerobic chemostat cultures. J. Biol. Chem. *282*, 10243–10251. https://doi.org/10.1074/jbc.m610845200.

Teusink, B., Passarge, J., Reijenga, C.A., Esgalhado, E., Van Der Weijden, C.C., Schepper, M., Walsh, M.C., Bakker, B.M., Van Dam, K., Westerhoff, H.V., and Snoep, J.L. (2000). Can yeast glycolysis be understood in terms of *in vitro* kinetics of the constituent enzymes? Testing biochemistry. Eur. J. Biochem. *267*, 5313–5329. https://doi.org/10.1046/j.1432-1327.2000.01527.x.

Thompson, A.L., and Cooney, G.J. (2000). Acyl-CoA inhibition of hexokinase in rat and human skeletal muscle is a potential mechanism of lipid-induced insulin resistance. Diabetes *49*, 1761–1765. https://doi.org/10.2337/diabetes.49.11.1761.

Tolias, K.F., and Cantley, L.C. (1999). Pathways for phosphoinositide synthesis. Chem. Phys. Lipids *98*, 69–77. https://doi.org/10.1016/s0009-3084(99)00019-5.

Trotter, P.J., Wu, W.I., Pedretti, J., Yates, R., and Voelker, D.R. (1998). A genetic screen for aminophospholipid transport mutants identifies the phosphatidylinositol 4-kinase, STT4p, as an essential component in phosphatidylserine metabolism. J. Biol. Chem. *273*, 13189–13196. https://doi.org/10.1074/jbc.273.21.13189.

Truong, D.M., and Boeke, J.D. (2017). Resetting the yeast epigenome with human nucleosomes. Cell *171*, 1508–1519.e13. https://doi.org/10.1016/j.cell.2017.10.043.

Tsai, H.J., and Wilson, J.E. (1996). Functional organization of mammalian hexokinases: both N- and C-terminal halves of the rat type II isozyme possess catalytic sites. Arch. Biochem. Biophys. *329*, 17–23. https://doi.org/10.1006/abbi.1996.0186.

Tschopp, J., and Schroder, K. (2010). NLRP3 inflammasome activation: the convergence of multiple signalling pathways on ROS production? Nat. Rev. Immunol. *10*, 210–215. https://doi.org/10.1038/nri2725.

Van Den Brink, J., Canelas, A.B., Van Gulik, W.M., Pronk, J.T., Heijnen, J.J., De Winde, J.H., and Daran-Lapujade, P. (2008). Dynamics of glycolytic regulation during adaptation of *Saccharomyces cerevisiae* to fermentative metabolism. Appl. Environ. Microbiol. *74*, 5710–5723. https://doi.org/10.1128/aem.01121-08.

Van Eunen, K., Bouwman, J., Daran-Lapujade, P., Postmus, J., Canelas, A.B., Mensonides, F.I.C., Orij, R., Tuzun, I., Van Den Brink, J., Smits, G.J., et al. (2010). Measuring enzyme activities under standardized in vivo-like conditions for systems biology. FEBS J. *277*, 749–760. https://doi.org/10.1111/j.1742-4658.2009.07524.x.

Van Eunen, K., Kiewiet, J.A.L., Westerhoff, H.V., and Bakker, B.M. (2012). Testing biochemistry revisited: how *in vivo* metabolism can be understood from *in vitro* enzyme kinetics. PLoS Comput. Biol. *8*, e1002483. https://doi.org/10.1371/journal.pcbi.1002483.

Van Hall, G. (2010). Lactate kinetics in human tissues at rest and during exercise. Acta. Physiol. *199*, 499–508. https://doi.org/10.1111/j.1748-1716.2010.02122.x.

Van Heerden, J.H., Wortel, M.T., Bruggeman, F.J., Heijnen, J.J., Bollen, Y.J., Planque, R., Hulshof, J., O'toole, T.G., Wahl, S.A., and Teusink, B. (2014). Lost in transition: startup of glycolysis yields subpopulations of nongrowing cells. Science *343*, 1245114. https://doi.org/10.1126/science.1245114.

Van Hoek, P., Van Dijken, J.P., and Pronk, J.T. (1998). Effect of specific growth rate on fermentative capacity of baker's yeast. Appl. Environ. Microbiol. *64*, 4226–4233. https://doi.org/10.1128/aem.64.11.4226-4233.1998.

Van Schaftingen, E., and Hers, H.G. (1981). Formation of fructose 2, 6-bisphosphate from fructose 1, 6-bisphosphate by intramolecular cyclisation followed by alkaline hydrolysis. Eur. J. Biochem. *117*, 319–323. https://doi.org/10.1111/j.1432-1033.1981.tb06339.x.

Verduyn, C., Postma, E., Scheffers, W.A., and Van Dijken, J.P. (1992). Effect of benzoic acid on metabolic fluxes in yeasts: a continuous culture study on the regulation of respiration and alcoholic fermentation. Yeast *8*, 501–517. https://doi.org/10.1002/yea.320080703.

Walker, B.J., Abeel, T., Shea, T., Priest, M., Abouelliel, A., Sakthikumar, S., Cuomo, C.A., Zeng, Q., Wortman, J., Young, S.K., and Earl, A.M. (2014). Pilon: an integrated tool for comprehensive microbial variant detection and genome assembly improvement. PLoS One *9*, e112963. https://doi.org/10.1371/journal.pone.0112963.

Warburg, O. (1925). The metabolism of carcinoma cells. J. Cancer Res. *9*, 148–163. https://doi.org/10.1158/jcr.1925.148.

Wilson, J.E. (1997). Homologous and heterologous interactions between hexokinase and mitochondrial porin: evolutionary implications. J. Bioenerg. Biomembr. *29*, 97–102. https://doi.org/10.1023/a:1022472124746.

Wilson, J.E. (2003). Isozymes of mammalian hexokinase: structure, subcellular localization and metabolic function. J. Exp. Biol. *206*, 2049–2057. https://doi.org/10.1242/jeb.00241.

Wolters, J.C., Ciapaite, J., Van Eunen, K., Niezen-Koning, K.E., Matton, A., Porte, R.J., Horvatovich, P., Bakker, B.M., Bischoff, R., and Permentier, H.P. (2016). Translational targeted proteomics profiling of mitochondrial energy metabolic pathways in mouse and human samples. J. Proteome. Res. *15*, 3204–3213. https://doi.org/10.1021/acs.jproteome.6b00419.

Woolford, J.L., and Baserga, S.J. (2013). Ribosome biogenesis in the yeast *Saccharomyces cerevisiae*. Genetics *195*, 643–681. https://doi.org/10.1534/genetics.113.153197.

Yoshida, S., Ohya, Y., Goebl, M., Nakano, A., and Anraku, Y. (1994). A novel gene, *STT4*, encodes a phosphatidylinositol 4-kinase in the PKC1 protein kinase pathway of *Saccharomyces cerevisiae*. J. Biol. Chem. *269*, 1166–1172. https://doi.org/10.1016/s0021-9258(17)42237-x.

Zeng, C., Aleshin, A.E., Chen, G., Honzatko, R.B., and Fromm, H.J. (1998). The roles of glycine residues in the ATP binding site of human brain hexokinase. Journal of Biological Chemistry *273* (2), 700–704.

Zhang, N., Osborn, M., Gitsham, P., Yen, K., Miller, J.R., and Oliver, S.G. (2003). Using yeast to place human genes in functional categories. Gene *303*, 121–129. https://doi.org/10.1016/s0378-1119(02)01142-3.

STAR★METHODS

KEY RESOURCES TABLE

REAGENT or RESOURCE	SOURCE	IDENTIFIER
Bacterial and virus strains		
Escherichia coli XL1-Blue	Agilent Technologies	Cat#200249
Chemicals, peptides, and recombinant proteins		
G418	Invivogen	Cat#ant-gn-5
Noursethricin	Jena bioscience	Cat#AB-101-10ML
Fluoroacetamide	Merck Sigma	Cat#128341-5G
Ampicillin	Merck Sigma	Cat#A9518-25G
Chloramphenicol	Merck Sigma	Cat# 29,231-5VL-F
Kanamycin	Merck Sigma	Cat# K1377-5G
Complete Protease Inhibitor Cocktail	Merck Sigma	Cat#11836145001
Phusion High-Fidelity DNA polymerase	Thermo Fisher Scientific	Cat#F549L
DreamTaq PCR Mastermix 2X	Thermo Fisher Scientific	Cat#K1072
T4 ligase buffer	Thermo Fisher Scientific	Cat#B69
T7 DNA ligase	New England Biolabs	Cat#M0318S
BsaI (Eco31I)	Thermo Fisher Scientific	Cat#ER0292
BsmBI	New England Biolabs	Cat#R0580S
FastDigest NotI	Thermo Fisher Scientific	Cat#FD0593
$NADP^+$	Merck Sigma	Cat#10128058001
glucose-6-phosphate dehydrogenase (EC1.1.1.49)	Merck Sigma	Cat#P4553-25UN
ATP	Merck Sigma	Cat#10127531001
Trehalose-6-phosphate	Merck Sigma	Cat#T4272-10MG
Glucose-6-phosphate	Merck Sigma	Cat#10127647001
Fructose-6-phosphate	Merck Sigma	Cat#F1502-500MG
AMP	Merck Sigma	Cat#01930-5G
NADH	Merck Sigma	Cat#10128023001
Aldolase (EC4.1.2.13)	Merck Sigma	Cat#A8811-200UN
Glycerol-3P-dehydrogenase (EC1.1.1.8) and triosephosphate isomerase (EC5.3.1.1)	Merck Sigma	Cat#G1881
Fructose 1,6-bisphosphate	Merck Sigma	Cat#F0752-10G
Glyceraldehyde-3-phosphate dehydrogenase (EC1.2.1.12)	Merck Sigma	Cat#G2267-1KU
3-phosphoglycerate kinase (EC2.7.2.3)	Merck Sigma	Cat#P7634-5KU
3-phosphoglyceric acid	Merck Sigma	Cat#P8877-1G
2,3-diphospho-glyceric acid	Merck Sigma	Cat#D9134-100MG
Enolase (EC4.2.1.11)	Merck Sigma	Cat#E6126-2.5KU
Pyruvate kinase (EC2.7.1.40)	Merck Sigma	Cat#P1506-5KU
L-lactate dehydrogenase (EC1.1.1.27)	Merck Sigma	Cat#L1254-5KU
2-phosphoglyceric acid	Merck Sigma	Cat#79470-250MG
ADP	Merck Sigma	Cat#A2754-1G
Phosphoenolpyruvate	Merck Sigma	Cat#P3637-1G
FM™ 4-64FX, fixable membrane stain	Thermo Fisher Scientific	Cat#34653
SYTOX Green Nucleic Acid Stain	Thermo Fisher Scientific	Cat#S7020
YeastBuster™ Protein Extraction Reagent	Novagen, via Merck Millipore	Cat#71186
TMT10plex™ Isobaric Label Reagent Set	Thermo Fisher Scientific	Cat#90110

(*Continued on next page*)

Continued

REAGENT or RESOURCE	SOURCE	IDENTIFIER
Sequencing Grade Modified Trypsin	Promega	Cat#V5111
Protease inhibitor cocktail	Sigma-Aldrich	Cat#P8215
Phosphatase inhibitor	Merck Sigma	Cat#524625
Iodoacetamide (IAA)	Merck Sigma	Cat#I1149
Ammonium bicarbonate (ABC)	Merck Sigma	Cat#09830
^{13}C-labelled peptides for absolute protein quantification (amino acid composition shown in Table S6)	Polyquant	N/A
Critical commercial assays		
Qubit dsDNA BR kit	Thermo Fisher Scientific	Cat#Q32850
YeaStar™ Genomic DNA kit	Zymo Research Corporation	Cat#D2002
GenElute™ Plasmid Miniprep Kit	Sigma-Aldrich	Cat#PLN350
Zymoclean Gel DNA Recovery kit	Zymo Research	Cat# D4002
GeneJET PCR Purification kit	Thermo Fisher Scientific	Cat#K0701
Qiagen Genomic-tip 100/G DNA isolation kit	Qiagen	Cat#10243
Qiagen Genomic DNA Buffer set	Qiagen	Cat#19060
BCA™ Protein Assay kit	Pierce, via Thermo Scientific	Cat#23225
D-Glucose assay kit	Megazyme	Cat#K-GLUC
Deposited data		
CEN.PK113-7D reference genome	(Salazar et al., 2017)	NCBI BioSample SAMN07328112 BioProject PRJNA393501
Crystal structure of human brain hexokinase type I	(Aleshin et al., 1998)	PDB: 1HKB
Crystal structure of human hexokinase II	(Nawaz et al., 2018)	PDB: 2NZT
Large-scale quantitative shotgun proteomics experiments	PXD025349, This paper.	http://www.ebi.ac.uk/pride/archive/projects/PXD025349
Whole genome sequencing data	This paper	NCBI bioproject PRJNA717746
COPASI model files	This paper	https://github.com/mvieiralara/humanizedyeast
Experimental models: Organisms/strains		
Saccharomyces cerevisiae, CEN.PK strain background	(Entian and Kötter, 2007)	CEN.PK113-7D; CBS 8340
Oligonucleotides		
All used oligonucleotides are listed in Table S8	N/A	N/A
Recombinant DNA		
All plasmids used and constructed are listed in Table S9	N/A	N/A
Software and algorithms		
PEAKS Studio X	Bioinformatics solutions Inc.	https://www.bioinfor.com/
Skyline Targeted Mass Spec Environment	MacCoss Lab Software	https://skyline.ms/project/home/software/Skyline/begin.view
Matlab2019b	The Mathworks Inc.	https://nl.mathworks.com/products/matlab.html
GraphPad Prism 9.3.0	GraphPad Software Inc.	https://www.graphpad.com/scientific-software/prism/
FlowJo 10.6.1	FlowJo, LLC	https://www.flowjo.com/
COPASI 4.23	(Hoops et al., 2006)	http://copasi.org/
PyMOL Molecular Graphics System 1.8.6	Schrödinger LLC	https://pymol.org/2/

(*Continued on next page*)

Continued

REAGENT or RESOURCE	SOURCE	IDENTIFIER
Magnolya copy number variation ‘	(Nijkamp et al., 2012)	https://sourceforge.net/projects/magnolya/
SAMtools	(Li et al., 2009)	http://www.htslib.org/
Pilon	(Walker et al., 2014)	https://github.com/broadinstitute/pilon
Integrative Genomics Viewer	Broad Institute	https://software.broadinstitute.org/software/igv/
ImageJ	NIH	https://imagej.nih.gov/ij RRID: SCR_002074
Other		
Uniprot database	UniProt Consortium	https://www.uniprot.org/
eQuilibrator database version 2.2.	(Flamholz et al., 2012)	https://equilibrator.weizmann.ac.il/
SBML kinetic model yeast glycolysis	(van Heerden et al., 2014)	https://jjj.bio.vu.nl/models/vanheerden1/
The common Repository of Adventitious Proteins	The Global Proteome Machine Organization	https://www.thegpm.org/crap/

RESOURCE AVAILABILITY

Lead contact

Further information and requests for resources and reagents should be directed to and will be fulfilled by the lead contact, Pascale Daran-Lapujade (P.A.S.Daran-Lapujade@tudelft.nl).

Materials availability

Yeast strains and plasmids generated in this study are available upon request. This study did not generate new unique reagents.

Data and code availability

The whole genome DNA sequencing data generated in this project are accessible at NCBI under bioproject PRJNA717746 and are publicly available as of the date of publication.

Mass spectrometric raw data have been deposited to the ProteomeXchange Consortium (http://proteomecentral.proteomexchange.org) via the PRIDE repository and are publicly available as of the date of publication with the dataset identifier PXD025349.

All data reported in this paper will be shared by the lead contact upon request.

COPASI models can be found at github.com/mvieiralara/humanizedyeast and is publicly available as of the date of publication.

Any additional information required to reanalyze the data reported in this paper is available from the lead contact upon request.

EXPERIMENTAL MODEL AND SUBJECT DETAILS

Yeast and *E. coli* strains

All yeast strains used and generated in this study are derived from the CEN.PK background (Entian and Kötter, 2007) and are listed in Table S7. Yeast strains were propagated at 30 ºC except otherwise indicated on YP medium containing 10g L^{-1} Bacto Yeast extract, 20 g L^{-1} Bacto Peptone or synthetic medium (SM) containing 5 g L^{-1} $(NH_4)_2SO_4$, 3 g L^{-1} KH_2PO_4, 0.5 g L^{-1} $MgSO_4 \cdot 7 \cdot H_2O$, and 1 mL L^{-1} of a trace elements and vitamin solution (Verduyn et al., 1992). Media were supplemented with 20 g L^{-1} glucose or galactose or 2% (v/v) ethanol. For the physiological characterization of the individual hexokinase complementation strains (Figure 4A) and to test the aldolase moonlighting function (Figures 4C and S8B), $(NH_4)_2SO_4$ was replaced with 6.6 g L^{-1} K_2SO_4 and 2.3 g L^{-1} urea to reduce acidification of the medium. Urea was filter sterilized and added after heat sterilization of the medium at 121°C. When indicated, 125 mg L^{-1} histidine was added. For solid media 2% (w/v) agar was added to the medium prior to heat sterilization. The pH of SM was adjusted to pH 6 by addition of 2 M KOH. For selection, YP medium was supplemented with 200 mg L^{-1} G418 (KanMX) or 100 mg L^{-1} nourseothricin (Clonat). For removal of the native yeast glycolysis cassette from the *sga1* locus the SM glucose (SMG) medium was supplemented with 2.3 g L^{-1} fluoracetamide to counter select for the *AmdS* marker present in the cassette (Solis-Escalante et al., 2013). Yeast strains were stored at −80°C after addition of 30% (v/v) glycerol to an overnight grown culture.

For plasmid propagation chemically competent *Escherichia coli* XL1-Blue (Agilent Technologies, Santa Clara, CA) cells were used which were grown in lysogeny broth (LB) supplemented with 100 mg L^{-1} ampicillin, 25 mg L^{-1} chloramphenicol or 50 mg L^{-1} kanamycin when required (Bertani, 1951, 2004). *E. coli* strains were stored at −80°C after addition of 30% (v/v) glycerol to an overnight grown culture.

Human myotube culture

Human myoblasts were obtained from orbicularis oculi muscle biopsies, which has previously been described (Koning et al., 2012). Briefly, a muscle biopsy was obtained from a healthy 60-year-old female donor, undergoing blepharoplasty, from which myoblasts were isolated as previously described. After 8 passages in culture, a subclone V49 that expressed Pax7, MyoD and Myogenin was used for the assays here described. Cells were maintained in high glucose Dulbecco's Modified Eagle's Medium (DMEM, Sigma-Aldrich/Merck) in the presence of L-glutamine, 20% fetal bovine serum (FBS, Life Technologies Gibco/Merck) and 1% penicillin/streptomycin (p/s, Sigma-Aldrich/Merck). For differentiation, cells were seeded on 10 cm dishes covered with polydimethylsiloxane (PDMS) gradients at 5,000 cells/cm^2. After reaching confluence, the medium was changed to DMEM in the presence of 2% FBS, 1% p/s, 1% Insulin-Transferrin-Selenium (Life Technologies Gibco/Merck) and 1% dexamethasone (Sigma-Aldrich/Merck). The presence of PDMS gradients allows cells to grow aligned, which in turn improves myotube maturity and functionality (Almonacid Suarez et al., 2019). Cells were harvested after 5 days in differentiation medium. In short, cells were washed twice with ice-cold Dulbecco's Phosphate Buffered Saline (DPBS, Gibco) and scraped in DPBS in the presence of Complete Protease Inhibitor Cocktail (Merck, 11836145001, 1:25 v/v after resuspension according to manufacturer's guidelines). Cell extracts were frozen at −80°C.

METHOD DETAILS

Growth rate determinations and laboratory evolution

For all growth experiments in shake flasks, 100 mL medium in a 500 mL shake flask was used except for the shake flask growth study with individual complementation strain for which 20 mL in a 100 mL volume shake flaks was used. Strains were incubated with constant shaking at 200 rpm and at 30°C unless stated otherwise. Strains were inoculated from glycerol stocks in YPD and grown overnight. This culture was used to inoculate the pre-culture (SMG) from which the exponentially growing cells were transferred to new shake flasks to start a growth study. Growth rates were determined from OD_{660} data by linear regression of the log-linear plots of OD_{660} versus time over at least six consecutive time-points in a range where the OD_{660} doubled twice, choosing the range to maximize the squared Pearson correlation coefficient (R^2).

Growth studies in microtiter plate were performed at 30°C and 250 rpm using a Growth Profiler 960 (EnzyScreen BV, Heemstede, The Netherlands). Strains from glycerol freezer stocks were inoculated and grown overnight in 10 mL YPD or YPGal medium in a 50 mL volume shake flask. This culture was used to inoculate a preculture in a 24-wells plate with a 1 mL working volume (EnzyScreen, type CR1424f) or a shakeflask with 15 mL of the medium of interest, which was grown until mid/late-exponential growth. From this culture the growth study was started in a 96-wells microtiter plate (EnzyScreen, type CR1496dl), with final working volumes of 250 μL and starting OD_{660} of 0.1–0.2. Microtiter plates were closed with a sandwich cover (EnzyScreen, type CR1296). Images of cultures were made at 30 min intervals. Green-values for each well were corrected for position in the plate using measurements of a culture of OD_{660} 5.05 of CEN.PK113-7D. Corrected green values were converted to OD-values based on 15-point calibrations, fitted with the following equation: OD-equivalent = $a \times GV(t) + b \times GV(t)^c - d$ in which GV(t) is the corrected green-value measured in a well at time point 't'. This resulted in curves with a = 0.0843, b = 5.35×10^{-8}, c = 4.40 and d = 0.42 for the data in Figures 1, 5, and S1 and a = 0.077, b = 1.66×10^{-7}, c = 3.62 and d = 1.61 for the data in Figures 4 and S8. Growth rates were calculated in a time frame where the calculated OD was between 2 and 10 in which OD doubled at least twice.

Adaptive laboratory evolution of IMX1814 and IMX1844 was performed in SMG at 30°C in 100 mL volume shake flasks with a working volume of 20 mL. Initially every 48 hours 200 μL of the culture was transferred to a new shake flask with fresh medium, after 22 transfers (approximately 170 generations) this was done every 24h. For both strains three evolution lines were run in parallel. At the end of the experiment single colony isolates were obtained by restreaking three times on YPD plates (Table S7D).

Molecular techniques, gene synthesis and Golden Gate plasmid construction

PCR amplification for cloning purposes was performed with Phusion High-Fidelity DNA polymerase (Thermo Fisher Scientific, Waltham, MA) according to the manufacturers recommendations except that the primer concentration was lowered to 0.2 μM. PCR products for cloning and Sanger sequencing were purified using the Zymoclean Gel DNA Recovery kit (Zymo Research, Irvine, CA) or the GeneJET PCR Purification kit (Thermo Fisher Scientific). Sanger sequencing was performed at Baseclear BV (Baseclear, Leiden, The Netherlands) and Macrogen (Macrogen Europe, Amsterdam, The Netherlands). Diagnostic PCR to confirm correct assembly, integration of the constructs and sequence verification by Sanger sequencing was done with DreamTaq mastermix (Thermo Fisher Scientific) according to the manufacturers recommendations. To obtain template DNA, cells of single colonies were suspended in 0.02 M NaOH, boiled for 5 min and spun down to use the supernatant. All primers used in this study are listed in Table S8. Primers for cloning purposes were ordered PAGE purified, the others desalted. To obtain gRNA and repair fragments the designed forward and reverse primers were incubated at 95°C for 5 min to obtain a double stranded piece of DNA. PCR products were separated in gels containing 1% agarose (Sigma) in Tris-acetate buffer (TAE). Genomic DNA from CEN.PK113-7D was extracted using the YeaStar™ Genomic DNA kit (Zymo Research Corporation, Irvine, CA, USA). Cloning of promoters, genes and terminators was done using Golden Gate assembly. Per reaction volume of 10 μl, 1 μl T4 buffer (Thermo Fisher Scientific), 0.5 μl T7 DNA ligase (NEB New England Biolabs, Ipswich, MA) and 0.5 μl BsaI (Eco31I) (Thermo Fisher Scientific) or BsmBI (NEB) was used and DNA parts were added in equimolar amounts of 20 fmol as previously described (Lee et al., 2015). First a plasmid backbone was constructed from parts of the yeast toolkit (Lee et al., 2015) using a kanamycin marker, *URA3* marker, bacterial origin of replication,

3′and 5′ *ura3* integration flanks and a *GFP* marker resulting in pGGKd002 (Table S9C). In a second assembly, the *GFP* gene in this plasmid was replaced by a transcriptional unit containing a *S. cerevisiae* promoter and terminator and a human glycolytic gene. The sequences of the human glycolytic genes were obtained from the Uniprot database, codon optimized for *S. cerevisiae* and ordered from GeneArt Gene Synthesis (Thermo Fisher Scientific). Genes were synthetized flanked with BsaI restriction sites to use them directly in Golden Gate assembly (Table S9A). The *PKL* gene which is a shorter splicing variant of *PKR* was obtained by amplifying it from the *PKR* plasmid pGGKp024 using primers containing BsaI restriction site flanks (Table S8G). *S. cerevisiae* promoters and terminators were PCR amplified from genomic DNA using primers flanked with BsaI and BsmBI restriction sites (Table S8A) (Boonekamp et al., 2018). The resulting PCR product was directly used for Golden Gate assembly. For long term storage of the fragments, the promoters and terminators were cloned into the pUD565 entry vector using BsmBI Golden Gate cloning resulting in the plasmids pGGKp025-048 listed in Table S9B. For the *HXK2* and *TEF2* promoters and *HXK2* and *ENO2* terminators already existing plasmids were used (Table S9B). For the construction of pUDE750 which was used as PCR template for the amplification of the *HsHK4* fragment used in IMX1814, first a dropout vector (pGGKd003) was constructed from the yeast toolkit parts pYTK002, 47, 67, 74, 82 and 84 (Table S9C). In this backbone, *ScHXK2p, HK4* and *ScHXK2t* were assembled as described above (Table S9E). Plasmid isolation was done with the GenElute™ Plasmid Miniprep Kit (Sigma-Aldrich, St. Louis, MO). Yeast transformations were performed according to the lithium acetate method (Gietz and Woods, 2002).

Construction of individual gene complementation strains

To enable CRISPR/Cas9 mediated gene editing, *Cas9* and the *NatNT1* marker were integrated in the *SGA1* locus of the minimal glycolysis strain IMX370 by homologous recombination, resulting in strain IMX1076 (Solis-Escalante et al., 2015). *Cas9* was PCR amplified from p414-*TEF1p-Cas9-CYC1t* and *NatNT1* from pUG-*natNT1* (Tables S8G and S9E) and 750 ng of both fragments were, after gel purification, used for transformation.

For the individual gene complementation study, 400 ng of the constructed plasmids containing the human gene transcriptional units (Table S9D) were linearized by digestion with NotI (FastDigest, Thermo Fisher Scientific) according to the manufacturer's protocol for 30 min and subsequently the digestion mix was directly transformed to IMX1076. The linearized plasmids were integrated by homologous recombination in the disrupted *ura3-52* locus of strain IMX1076 and the transformants were plated on SMG. After confirmation of correct integration by PCR (Table S8B), in a second transformation the orthologous yeast gene (or genes, in case of *PFK1* and *PFK2*) was removed using CRISPR/Cas9 according to the protocol of Mans et al. (Mans et al., 2015). Since only the yeast gene and not the human ortholog should be targeted, the gRNAs were designed manually (Table S8D). For deletion of *FBA1*, *GPM1*, and *PFK1* and *PFK2,* the plasmids containing the gRNA were preassembled as previously described (Mans et al., 2015) using Gibson assembly and a PCR amplified pROS13 backbone containing the KanMX marker (Tables S8D and S9F). For *HXK2* deletion, the double stranded gRNA and a PCR amplified pMEL13 backbone were assembled using Gibson assembly (Table S8D). The constructed plasmids were verified by PCR. The rest of the gRNA plasmids for yeast gene deletion were assembled *in vivo* in yeast and were not stored as individual plasmid afterwards. For the *in vivo* assembly approach the strains were co-transformed with 100 ng of the PCR amplified backbone of pMEL13 (Tables S8D and S9F), 300 ng of the double stranded gRNA of interest (Table S8D) and 1 μg repair fragment to repair the double-stranded break (Table S8E). For pre-assembled plasmids, strains were co-transformed with 0.6–1 μg of plasmid (Table S9F) and 1 μg repair fragment (Table S8E). Transformants were plated on YPD + G418 and for the *HsHK1-HK3* strains on YPGal + G418. Successful gene deletion was confirmed with diagnostic PCR (Table S8B, Figure S14). gRNA plasmids were afterwards removed by several restreaks on non-selective medium. To test if the complementation was successful, the strains were tested for growth in SMG. For *HsHK2,* three complementation strains were made. IMX1690 (*pScPDC1-HsHK2)* and IMX1873 (*pScHXK2-HsHK2*) which were grown on glucose medium and contain a mutation in *HsHK2* and IMX2419 (*pScPDC1-HsHK2)* which was never exposed to glucose and does not contain mutations. Similarly for *HsHK1,* complementation strain IMX1689 was not grown on glucose, after growth on glucose mutations occurred and strains IMS1137, IMS1140 and IMS1143 were stocked. *HsHK4* was also expressed both with the *ScHXK2* and *ScPDC1* promoter, resulting in IMX1874 and IMX1334 respectively (Tables S7A and S7B). An overview of the workflow is provided in Figure S1. To test for the occurrence of mutations, the human gene transcriptional units were PCR amplified using the primers listed in Table S8 and sent for Sanger sequencing.

Full human glycolysis strain construction

For the construction of the strains containing a full human glycolysis, the transcriptional units of the *HsHK2, HsHK4, HsGPI, HsPFKM, HsALDOA, HsTPI1, HsGAPDH, HsPGAM2, HsENO3,* and *HsPKM1* gene were PCR amplified from the same plasmids as were used for the individual gene complementation using primers with flanks containing synthetic homologous recombination (SHR) sequences (Tables S8C and S9D). For the *HsHK2* and *HsHK4* gene for which pUDE750 and pUDI207 were used as template, which contain the Sc*HXK2* promoter and terminator. An overview of the promoters used for the human gene expression is provided in Table S2. The yeast *PDC1* and *ADH1* genes were amplified with their corresponding promoter and terminator regions from genomic DNA from CEN.PK113-7D (Table S7E). The fragments were gel purified and the fragments were assembled in the *CAN1* locus of strain IMX589 by *in vivo* assembly. 160 fmol per fragment and 1 μg of the pMEL13 plasmid targeting *CAN1* was used. Transformation mix was plated on YPD + G418 and correct assembly was checked by PCR and resulted in strain IMX1658. In a second transformation, the cassette in the *SGA1* locus containing the native *S. cerevisiae* glycolytic genes and the *AmdS* marker was removed. To this end IMX1658 was transformed with 1 μg of the gRNA plasmid pUDE342 (Table S9F) and 2 μg repair fragment (counter select oligo)

(Table S8E) and plated on SMG medium with fluoracetamide to counter select for the *AmdS* marker. From the resulting strain the pUDE342 plasmid was removed and it was stored as IMX1668. To replace the *HsHK4* gene with *HsHK2,* the *HsHK2* gene was PCR amplified from pGGKp002 using primers flanked with sequences homologous to the *ScHXK2* promoter and terminator to allow for recombination (Table S8G). IMX1668 was co-transformed with this fragment and pUDR387 containing the gRNA targeting the *HsHK4* gene and the cells were plated on YPD + G418 (Table S9F). After confirmation of correct integration by PCR and plasmid removal, the strain was stored as IMX1785. The pUDR387 gRNA plasmid was constructed with Gibson Assembly from a pMEL13 backbone and double stranded *HsHK4* gRNA fragment (Table S8D). To make the constructed yeast strains prototrophic, the *ScURA3* marker was PCR amplified from CEN.PK113-7D genomic DNA using primers with flanks homologous to the *TDH1* region (Table S8G) and integrated in the *tdh1* locus of IMX1785 and IMX1668, by transforming the strains with 500 ng of the fragment and plating on SMG. This resulted in IMX1844 and IMX1814 respectively. These strains were verified by whole genome sequencing (Table S3) and the ploidy was verified (Figure S15). IMX2418 (*Hs*Gly *HK2* strain without mutation in *HsHK2*) was constructed by transforming IMX1814 with pUDR387 and the *HsHK2* fragment amplified as described above. The cells were plated on YPGal + G418 and later restreaked on YPGal plates to remove the plasmid. For the overexpression of *HsALDOA, HsPGAM2* and *HsHK2*/*HsHK4* resulting in IMX2005 and IMX2006*,* the expression cassettes were PCR amplified from pUDI141, pUDI150, pUDI134 and pUDI136 respectively using primer sets 12446/12650, 12467/14542 and 14540/14541 (Tables S8C and S9D). IMX1844 and IMX1814 were transformed with 160 fmol per fragment and 1 μg of the plasmid pUDR376 containing a gRNA targeting the X2 locus (Mikkelsen et al., 2012) and plated on SMG-acetamide plates. To obtain the reference strain IMX1821 which contains a yeast glycolysis cassette integrated in *CAN1,* the pUDE342 plasmid was removed from the previously described strain IMX605 (Kuijpers et al., 2016) and the *URA3* fragment was integrated in *tdh1* in the manner as described above*.* An overview of strain construction is provided in Figure S16.

Note that the yeast strain for pathway swapping contains the native glycolysis and the fermentation genes (*ScPDC1* and *ScADH1*) clustered in a single locus. In the swapping approach, this locus is completely removed. As deletion of *ScPDC1* and *ScADH1* is lethal for yeast, they were reintroduced with the human glycolysis genes.

STT4 reverse engineering

The single nucleotide polymorphisms (SNPs) which were found in the *STT4* gene of evolved strains IMS0990 and IMS0992 resulting in amino acid changes G1766R and F1775I respectively, were introduced in the *STT4* genes of the non-evolved strains IMX1814, IMX1844 and IMX1822 using CRISPR/Cas9 editing (Mans et al., 2015) (Table S7D). Two gRNA plasmids pUDR666 and pUDR667 were constructed using Gibson Assembly of a backbone amplified from pMEL13 (Tables S8D and S9F) and a gRNA fragment consisting of oligo 16748 + 16749 and 16755 + 16756 respectively (Table S8D). For introduction of the G1766R mutation, strains were transformed with 500 ng of pUDR666 and 1 μg of repair fragment (oligo 16750 + 16751) and for introduction of F1775I with 500 ng of pUDR667 and 1 μg of repair fragment (oligo 16757 + 16758) (Tables S8E and S9F). Strains were plated on YPD + G418 and introduction of the mutation was verified by Sanger sequencing. The control strain IMX1822 containing the native yeast minimal glycolysis in the *SGA1* locus originates from strain IMX589 (Kuijpers et al., 2016). From this strain the *AmdS* marker was removed by transforming the strain with 1 μg repair fragment (oligo 11590 + 11591) and 300 ng of a gRNA fragment (oligo 11588 + 11589, Table S8D) targeting *AmdS* and 100 ng of backbone amplified from pMEL10 resulting in a *in vivo* assembled gRNA plasmid. After removal of the plasmid by restreaking on non-selective medium, this strain, IMX1769, was made prototrophic by integrating *ScURA3* in *tdh1* (Tables S8G and S7E), resulting in IMX1822*.*

Visualization of hexokinase mutants

Sequencing of the *HsHK1* and *HsHK2* carrying strains showed the presence of mutations in all strains after growth on glucose. All found mutations were mapped unto the protein sequence and visualized on the structural model with PDB code 1HKB (Aleshin et al., 1998) for *Hs*HK1 and 2NZT (Nawaz et al., 2018) for *Hs*HK2 using the PyMOL Molecular Graphics System, version 1.8.6 (Schrödinger LLC).

Computational modeling of human hexokinase complementation

Native human hexokinase complementation strains were simulated with the use of a previously published computational model of yeast glycolysis (van Heerden et al., 2014). The SBML version of the model was downloaded from *jjj.bio.vu.nl/models/vanheerden1* and imported into COPASI (software version 4.23) (Hoops et al., 2006). All concentrations in the model are expressed as mM and time in minutes. Equilibrium constants (K_{eq}'s) were obtained from Equilibrator (V 2.2) (Flamholz et al., 2012) at pH 6.8 and ionic strength 360 mM (van Eunen et al., 2010). The V_{max}'s from the MG strain from Kuijpers et al. (2016) (Kuijpers et al., 2016) were initially incorporated to create a control strain. For the complementation strains, the kinetic equation of hexokinase was first adapted to include competitive terms from G6P and ADP inhibition and trehalose 6-phosphate inhibition of the human enzymes was disregarded based on our kinetic results. Mammal kinetic parameters were obtained from (Grossbard and Schimke, 1966). *Hs*HK1 and *Hs*HK2 glycolysis models were subsequently obtained by incorporating the hexokinase V_{max} measured from strains IMX1689 and IMX2419, respectively. Steady-state fluxes were calculated with the integration of ordinary differential equations. Flux control coefficients (FCC) and response coefficients (R) were calculated in COPASI under Metabolic Control Analysis and Sensitivities according to Equations 1 and 2 below, respectively. J_{ss} represents a steady-state flux, for which the glucose uptake flux was used. $V_{max\ i}$ represents the V_{max}

while P_i stands for a kinetic parameter of an enzyme 'i' in the pathway. Summation theorem was verified for FCC calculations (Fell, 1992).

$$FCC^i = \frac{\partial \ln J_{ss}}{\partial \ln V_{maxi}} \quad \text{(Equation 1)}$$

$$R^i = \frac{\partial \ln J_{ss}}{\partial \ln P_i} \quad \text{(Equation 2)}$$

The human hexokinases *Hs*HK1 and *Hs*HK2 can only complement the yeast hexokinase upon mutations in the vicinity of the catalytic pocket. Therefore we aimed at investigating (1) why the native human hexokinases cannot complement the yeast hexokinase and (2) how mutations of the human hexokinases allow growth. In order to tackle these questions we have taken a computational modeling approach starting from the yeast glycolysis model from van Heerden et al. (van Heerden et al., 2014) which is based on the model by Teusink et al. (Teusink et al., 2000) Since growth cannot be directly addressed based exclusively on a metabolic model such as the glycolysis model, our approach was to evaluate changes in glycolytic fluxes as an index with a direct causal relation to the growth rate of cells. Starting from the van Heerden model (van Heerden et al., 2014) a step-by-step procedure was followed, resulting in the 5 models described in Figure S17. All models used in the present study can be found at github.com/mvieiralara/humanizedyeast.

First, the Equilibrium constants of the model were updated based on values computed with Equilibrator (http://equilibrator.weizmann.ac.il/) at pH 6.8 and ionic strength 360 mM (van Eunen et al., 2010). The list of Equilibrium constants used can be found in the table below. These values are necessary to calculate the reverse V_{max} when only the forward V_{max} was measured or vice-versa. To make the model more robust to changes and still physiologically relevant, the steady-state concentration of intracellular free phosphate was set as 30 mM. This value is within the range of 10-75 mM reported by Van Eunen et al. (2010) (van Eunen et al., 2010), and consistent with the fact that the growth medium contained 22 mM phosphate. These proposed changes were necessary for the MG model (M5) to reach a stable steady-state.

Equilibrium constants (K_{eq}) for the forward reactions.

Enzyme	Equilibrator*
HK	548
PGI	0.36
FBA	0.00014
TPI	0.11
GAPDH	0.103
PGK	1,700
PGAM	0.184
ENO	5.190
PYK	88,000
ADH (reverse reaction)	0.00016
AK	0.471
G3PDH	43,000

*No K_{eq} used for PFK and PDC in the van Heerden model, as these reactions were treated as irreversible.

From Teusink et al. (Teusink et al., 2000), we have the following relationship for volume and protein content in yeast: 3.75 μL cell vol/mg protein (= $3.75 \cdot 10^{-6}$ L/mg protein). The measured V_{max}'s for the IMX372 strain (Minimal Glycolysis, MG) are shown below both in μmol/(min • mg prot) as well as the mM/min equivalents calculated based on the intracellular volume (tables below). For PGI and GAPDH the forward V_{max}'s were calculated from the measured reverse V_{max}'s based on the Haldane relation. The table below summarizes the V_{max}'s used for the simulations followed by the calculations performed according to the Haldane relationship. For GAPDH, the following Haldane relationship applies:

$$K_{eq} = \frac{V_f K_{mBPG} K_{mNADH}}{V_r K_{mNAD} K_{mGAP} K_{mPi}}$$

a. K_mBPG = 0.0098 mM, K_mNADH = 0.06 mM, K_mNAD = 0.09 mM, K_mGAP = 0.21 mM, K_mPi = 1 mM, K_{eq} = 0.103 mM^{-1}

b. V_r = 1135 mM/min
c. V_f = 3758 mM/min

For PGI, the following Haldane relationship applies:

$$K_{eq} = \frac{V_f K_{mF6P}}{V_r K_{mG6P}}$$

a. K_mF6P = 0.3 mM, K_mG6P = 1.4 mM, K_{eq} = 0.36
b. V_r = 897 mM/min
c. V_f = 1507 mM/min

V_{max} values used in the simulations (input as mM/min).

Enzyme	MG strain (IMX372)		HK2 compl. strain (IMX2419)#		HK1 compl. strain (IMX1689)#	
	μmol/(min • mg prot)	mM/min	μmol/(min • mg prot)	mM/min	μmol/(min • mg prot)	mM/min
HK	1.32	351	0.567	151	0.526	140
PGI (rev)	3.37	897	3.37	897	3.37	897
PGI (for)*	5.66	1507	5.66	1507	5.66	1507
PFK	0.72	191	0.72	191	0.72	191
FBA	1.60	428	1.60	428	1.60	428
GAPDH (rev)	4.26	1135	4.26	1135	4.26	1135
GAPDH (for)*	14.10	3758	14.1	3758	14.10	3758
PGK (rev)	9.46	2522	9.46	2522	9.46	2522
GPM	9.66	2576	9.66	2576	9.66	2576
ENO	1.85	493	1.85	493	1.85	493
PYK	8.90	2372	8.90	2372	8.90	2372
ADH	1.37	365	1.37	365	1.37	365
PDC	1.49	398	1.49	398	1.49	398

#Assumed to be the same as the MG strain IMX372, except for hexokinase in the complementation strains.
*Calculated according to the Haldane relationship.

A comparison between the original van Heerden model (M1) and the model with updated K_{eq}'s and free phosphate concentrations (M1.2) shows no effect on steady-state fluxes and small effects on steady-state metabolite concentrations, with the exception of TRIO (the sum of GAP and DHAP) and NADH (Figures S18A and S18B). This can be explained by a 18-fold difference in the K_{eq} for GAPDH used for model M1.2 when compared to M1.

The equation for yeast hexokinase (below) followed a generic bisubstrate equation with random binding order. A similar equation was used for the human hexokinase, with G6P binding competitive with ATP and ADP and parameters (Table below) as described below.

$$V_{YeastHK} = \frac{\frac{V_{max}}{K_{m,Glc_i}} \cdot \left([Glc_i] \cdot [ATP] - \frac{[G6P] \cdot [ADP]}{K_{eq}} \right)}{\left(1 + \frac{[Glc_i]}{K_{m,Glc_i}} + \frac{[G6P]}{K_{m,G6P}} + \frac{[G6P]}{K_{i,G6P}} \right) \cdot \left(1 + \frac{[ATP]}{K_{m,ATP}} + \frac{[ADP]}{K_{m,ADP}} \right)}$$

$$V_{HumanHK1/HK2} = \frac{\frac{V_{max}}{K_{m,Glc_i} \cdot K_{m,ATP}} \cdot \left([Glc_i] \cdot [ATP] - \frac{[G6p] \cdot [ADP]}{K_{eq}} \right)}{\left(1 + \frac{[Glc_i]}{K_{m,Glc_i}} + \frac{[G6P]}{K_{m,G6P}} + \frac{[G6P]}{K_{i,G6P}} \right) \cdot \left(1 + \frac{[ATP]}{K_{m,ATP}} + \frac{[ADP]}{K_{m,ADP}} + \frac{[G6P]}{K_{i,G6p}} \right)}$$

Equation yeast hexokinase.

- K_iG6P: proxy for trehalose 6-P (T6P) inhibition, competitive for glucose (van Heerden et al., 2014)

Equation human hexokinase.

- K_iG6P: glucose 6-P inhibition, competitive for ATP (Grossbard and Schimke, 1966)
- K_iADP: ADP inhibition. This inhibition is described to be mixed, but for simplicity only the competitive term was included in the rate equation (Grossbard and Schimke, 1966)

Differences between yeast and hexokinase kinetic parameters.

Parameter	*Sc*HXK (van Heerden et al., 2014)	*Hs*HK2 (Grossbard and Schimke, 1966)	*Hs*HK1 (Grossbard and Schimke, 1966)
K_m ATP (mM)	0.15	0.78	0.4
K_m Glucose (mM)	0.08	0.23	0.045
K_m ADP (mM)	0.23	2.2	0.62
K_m G6P (mM)	30	0.16	0.21
K_i ADP (mM)	–	5.4	2.0
K_i G6P (mM)	0.07 (K_i T6P)	0.021 (native)[#] 0.063 (mutated)*	0.026 (native)[#] 0.21 (mutated)*

[#]Literature reference values.
*Estimated from the IC_{50} measurements from strain IMX1690 for *Hs*HK2 and from strain IMS1137 for *Hs*HK1.

Figures S18C–S18G shows a comparison between the four generated models (M1.2, M5, M6 and M7). Fluxes, metabolite concentrations and the control of glucose uptake and ethanol fluxes are depicted. When either human hexokinase 2 or 1 were added to the model (M6 and M7), steady-state glycolytic fluxes (quantified as the flux through the glucose transporter GLT, and alcohol dehydrogenase ADH) were around one-third of those in the WT and MG models (M1.2 and M5) (Figure S18C). In the human hexokinase models (M6 and M7), predicted ATP concentrations at steady state were around 50% lower than in the WT and MG controls (Figure S18D). A higher flux control coefficient of the human hexokinases on the glycolytic fluxes in models M6 and M7 was observed when compared to the control models (Figures S18E–S18G). This was accompanied by higher flux control at the PFK and GAPDH nodes, which is compensated by lower flux control by glucose uptake (GLT) and ATP utilization (ATPase). Figure S18 Panel G shows that the human hexokinase models differ from the WT and MG in terms of the distribution of glycolytic intermediates. An apparent bottleneck at hexokinase in the human hexokinase models (M6 and M7 can be recognized from the accumulation of more intracellular glucose (Glc_i) than in the control models.

To evaluate whether trehalose-6P (T6P) would inhibit *Hs*HK2, the activity of the enzyme was measured in the presence of 1 mM T6P. This inhibited both *Hs*HK2 (native) and *Hs*HK2^{L776F} (mutated) by roughly 50% (Figure S4B). We used this information to evaluate whether T6P inhibition would have a further impact on the glycolytic fluxes of the *Hs*HK2 complementation strain with the use of model M6. The IC_{50}T6P for human hexokinase 2 can be estimated to be 1 mM at the experimental conditions used. Assuming competitive inhibition, we can estimate the range of K_iT6P for the human enzyme given the following equation:

$$IC_{50} = K_i\left(1 + \frac{[S]}{K_m}\right)$$

Given that the concentration of glucose used in the assay is 1 mM and its K_m is 0.23 mM, the term 1+ [S]/K_m can be approximated to 5, which means that the K_i would be roughly IC_{50}/5, or 0.2 mM. This is 3 times higher than the Ki for T6P reported for the yeast hexokinase in the van Heerden model (0.07 mM). Including this parameter in the human hexokinase equation (representing a competitive term in the glucose binding pocket) results in no changes in glycolytic fluxes. A parameter scan performed with the *Hs*HK2 model (M6) shows little to no effect of the parameter within this range (Figure S18H).

Construction of *Δhxk1Δhxk2* strain IMX165 and control strain IMX2015

The *Δhxk1Δhxk2* strain IMX165 which was used as control in the invertase assay was constructed in three steps. The *HXK1* and *HXK2* deletion cassettes were PCR amplified from pUG73 and pUG6 respectively using the primers listed in Table S8F. First, *HXK1* was removed from CEN.PK102-12A by transformation with the *HXK1* deletion cassette containing the *Kluyveromyces lactis LEU2* marker flanked with *loxP* sites and *HXK1* recombination flanks resulting in strain IMX075. To remove the *LEU2* marker from this strain, it was transformed with the plasmid pSH47 containing the galactose inducible Cre recombinase (Güldener et al., 1996). Transformants were plated on SMG with histidine and were transferred to YPGal for Cre recombinase induction to remove *LEU2,* resulting in strain IMS0336. Subsequently, this strain was transformed with the *HXK2* deletion cassette containing the *KanMX* marker flanked with *LoxP* sites and *HXK2* recombination flanks, resulting in IMX165. IMX2015 was constructed as control strain for the characterization of the human hexokinase complementation strains. In this strain Sc*HXK2* is expressed with the p*PDC1* promoter instead of the native *HXK2* promoter. *pPDC1* was PCR amplified from genomic DNA from CEN.PK113-7D with primer 14,670 and 14,671 containing *HXK2* recombination flanks. 500 ng of this fragment was transformed to IMX1076 together with 800 ng of pUDE327 containing a gRNA targeting the *HXK2* promoter (Table S9F).

Illumina whole genome sequencing

Genomic DNA for sequencing was isolated with the the Qiagen 100/G kit according to the manufacturer's description (Qiagen, Hilden, Germany) and library preparation and sequencing was done as described previously using Illumina Miseq sequencing (Illumina, San Diego, CA) (Boonekamp et al., 2018). Data were aligned to a CEN.PK113-7D reference (Salazar et al., 2017) and data were further processed using SAMTools (Li et al., 2009), and SNPs were determined using Pilon (Walker et al., 2014). The output was visualized using the Integrative Genomics Viewer and chromosome copy numbers were determined using Magnolya (Nijkamp et al., 2012). A list of mutations is provided in Table S3. For the mutation found in the *SBE2* gene which is involved in bud growth, it is unlikely to have an effect since it has a functionally redundant paralog *SBE22* (Santos and Snyder, 2000). No abnormalities were observed under the microscope. The sequencing data generated in this project are accessible at NCBI under bioproject PRJNA717746.

Quantitative aerobic batch cultivations

Quantitative characterization of strains IMX1821, IMX1814 and IMX1844 was done in 2 L bioreactors with a working volume of 1.4 L (Applikon, Schiedam, The Netherlands). The cultivation was done in synthetic medium supplemented with 20 g L^{-1} glucose, 1.4 mL of a vitamin solution (Verduyn et al., 1992) and 1.4 mL of 20% (v/v) Antifoam emulsion C (Sigma, St. Louise, USA). During the fermentation 0.5 mL extra antifoam was added when necessary. The salt and antifoam solution were autoclaved separately at 121°C and the glucose solution at 110°C for 20 min. During the fermentation the temperature was kept constant at 30°C and the pH at 5 by automatic addition of 2 M KOH. The stirring speed was set at 800 rpm. The medium was flushed with 700 mL min^{-1} of air (Linde, Gas Benelux, The Netherlands). For preparation of the inoculum, freezer stocks were inoculated in 100 mL YPD and grown overnight. From this culture the pre-culture was inoculated in 100 mL SMG which was incubated till mid-exponential growth phase. This culture was used to inoculate the inoculum flasks which were incubated till OD 4.5. The cells were centrifuged for 10 min at 3000g and the pellet was suspended in 100 mL demineralized water and added to the fermenter to start the fermentation with an OD of 0.25–0.4.

Biomass dry weight determination was done as previously described (Verduyn et al., 1992) by filtering 10 mL of culture on a filter with pore-size 0.45 mm (Whatman/GE Healthcare Life Sciences, Little Chalfont, United Kingdom) in technical duplicate. For extracellular metabolite analysis 1 mL of culture was centrifuged for 3 min at 20000g and the supernatant was analyzed using high-performance liquid chromatography (HPLC) using an Aminex HPX-87H ion-exchange column operated at 60°C with 5 mM H_2SO_4 as the mobile phase with a flow rate of 0.6 mL min^{-1} (Agilent, Santa Clara). Off-gas was cooled in a condenser and dried with a Perma Pure Dryer (Perma Pure, Lakewood, NJ), O_2 and CO_2 concentrations were measured using an NGA 2000 Rosemount gas analyzer (Emerson, St. Louis, MO). The OD_{660} was measured with a Jenway 7200 spectrophotometer (Jenway, Staffordshire, UK) at 660 nm. Per strain at least two independent fermentations were performed. The carbon balances for all reactors closed within 5%.

Growth rates (μ_{max}) were determined from OD_{660} data by linear regression of the log-linear plots of OD_{660} versus time over at least six consecutive time-points in a range where the OD_{660} doubled twice, choosing the range to maximize the squared Pearson correlation coefficient (R^2). Dry weights for all time points were estimated through a linear correlation of OD_{660} and dry weight based on the dry-weights from the same experiment. Molar yields for the products biomass, CO_2, ethanol, glycerol and acetate on glucose were determined as the slope of the correlation of the product concentration against glucose concentration during the exponential phase (the same time period used for growth rate determination). The specific glucose uptake rate (q_S) was determined by dividing the growth rate through the biomass yield on glucose. Specific product production rates and the oxygen consumption rate was determined by multiplying the molar yields with the specific glucose uptake rate.

Sample preparation and enzymatic assays for comparison of yeast and humanized yeast samples

Yeast samples were prepared as previously described (Postma et al., 1989), from exponentially growing cultures (62 mg dry weight per sample) from bioreactor main activity determinations and for testing of allosteric effectors and for comparison of the evolved strains from shake flask. Sonication was used for cell-free extract preparation except for the hexokinase measurements (Figures 2, S2, and S3) where fast-prep was used. All determinations were performed at 30°C and 340 nm (εNAD(P)H at 340 nm/6.33 mM^{-1}). In most cases glycolytic V_{max} enzyme activities were determined in 1 mL reaction volume (in 2 mL cuvettes), using a Hitachi model U3100 spectrophotometer, using previously described assays (Jansen et al., 2005), except for phosphofructokinase activity which was determined according to Cruz et al.(Cruz et al., 2012). When required extracts were diluted in phosphate buffer with the exception of TPI measurements for which the extracts were diluted in water (Postma et al., 1989).

Briefly for each enzyme assays contained:

Hexokinase (HXK; EC2.7.1.1) – 50 mM Imidazole-HCl (pH 7.6), 1 mM $NADP^+$, 10 mM $MgCl_2$, 10 mM Glucose, 1.8 U/mL glucose-6-phosphate dehydrogenase (EC1.1.1.49), and 1 mM ATP as start reagent.

Phosphoglucose isomerase (GPI; EC5.3.1.9) – 50 mM Tris-HCl (pH 8.0), 5 mM $MgCl_2$, 0.4 mM $NADP^+$, 1.8 U/mL glucose-6-phosphate dehydrogenase (EC1.1.1.49), and 2 mM fructose 6-phosphate as start reagent.

Phosphofructokinase (PFK; EC2.7.1.11) – 50 mM Imidazole-HCl (pH 7.0), 1 mM AMP, 5 mM $MgCl_2$, 0.15 mM NADH, 0.45 U/mL aldolase (EC4.1.2.13), 0.6 U/mL glycerol-3P-dehydrogenase (EC1.1.1.8), 1.8 U/mL triosephosphate isomerase (EC5.3.1.1), 0.5 mM Fructose-6-phosphate, and 1 mM ATP as start reagent.

Aldolase (ALDO; EC4.1.2.13) – 50 mM Tris-HCl (pH 7.5), 100 mM KCl, 0.15 mM NADH, 0.6 U/mL glycerol-3P-dehydrogenase (EC1.1.1.8), 1.8 U/mL triosephosphate isomerase (EC5.3.1.1), and 2 mM fructose 1,6-bisphosphate as start reagent.

Triosephosphate isomerase (TPI, EC5.3.1.1) – 200 mM Triethanolamine (pH 8.2), 0.15 mM NADH, 5 U/mL Glycerol 3P-dehydrogenase (EC1.1.1.8), 17.4 mM Glyceraldehyde-3-phosphate as start reagent.

Glyceraldehyde-3-phosphate dehydrogenase (GAPDH; EC1.2.1.12) – 100 mM Triethanolamine-HCl (pH 7.6), 1 mM ATP, 1 mM EDTA, 1.5 mM $MgSO_4$, 0.15 mM NADH, 16.5 U/mL 3-phosphoglycerate kinase (EC2.7.2.3), and 5 mM 3-phosphoglyceric acid as start reagent.

3-phosphoglycerate kinase (PGK; EC2.7.2.3) – 100 mM Triethanolamine-HCl (pH 7.6), 1 mM ATP, 1 mM EDTA, 1.5 mM $MgSO_4$, 0.15 mM NADH, 8 U/mL glyceraldehyde-3-phosphate dehydrogenase (EC1.2.1.12), and 5 mM 3-phosphoglyceric acid as start reagent.

Phosphoglycerate mutase (PGAM; EC5.4.2.1) – 100 mM Triethanolamine-HCl (pH 7.6), 1.5 mM $MgSO_4$, 0.15 mM NADH, 10 mM ADP, 1.25 mM 2,3-diphospho-glyceric acid, 6.3 U/mL enolase (EC4.2.1.11), 13 U/mL pyruvate kinase (EC2.7.1.40), 11.3 U/mL L-lactate dehydrogenase (EC1.1.1.27), and 5 mM 3-phosphoglyceric acid as start reagent.

Enolase (ENO; EC4.2.1.11) – 100 mM Triethanolamine-HCl (pH 7.6), 1.5 mM $MgSO_4$, 0.15 mM NADH, 10 mM ADP, 9 U/ml pyruvate kinase (EC2.7.1.40), 11.3 U/mL L-lactate dehydrogenase (EC1.1.1.27), and 1 mM 2-phosphoglyceric acid as start reagent.

Pyruvate kinase (PK; EC2.7.1.40) – 100 mM Cacodylic Acid (pH 6.2), 100 mM KCl, 10 mM ADP, 1 mM fructose 1,6-bisphosphate, 25 mM $MgCl_2$, 0.15 mM NADH, 8 U/mL L-lactate dehydrogenase (EC1.1.1.27) and 2 mM phosphoenolpyruvate as start reagent.

To increase throughput, the specific activities of the evolved strains and the glucose, ATP and ADP dependency of the hexokinase complementation strains (Figures S2C–S2E) were assayed using a TECAN infinite M200 Pro. (Tecan, Männedorf, Switzerland) microtiter plate reader. Samples were prepared manually in microtiter plates (transparent flat-bottom Costar plates; 96 wells) using a reaction volume of 300 μL per well. The assays were the same as for the cuvette-based assays. For determination of glucose-6-phosphate inhibition of hexokinase, cell extracts were prepared in Tris-HCl buffer (50 mM, pH 7.5) to limit phosphate concentrations, which could influence glucose-6-phosphate inhibition. For these measurements an alternative enzyme assay coupled by pyruvate kinase and lactate dehydrogenase was used based on (Rijksen and Staal, 1977), buffer and metabolite concentrations were kept the same as the yeast hexokinase assay.

Alternative assay hexokinase (HXK; EC2.7.1.1) – 50 mM Imidazole-HCl (pH 7.6), 10 mM $MgCl_2$, 0.15 mM NADH, 0.5 mM Phosphoenolpyruvate, 1 mM ATP, 2 U/mL Pyruvate Kinase (EC2.7.1.40), 4 U/ml L-lactate dehydrogenase (EC1.1.1.27) and 10 mM Glucose as start reagent, supplemented with various glucose-6-phosphate concentrations.

The reported data are based on at least two independent biological replicate samples, with at least two analytic replicates per sample per assay, including two different cell-free extract concentrations. The protein concentration was determined using the Lowry method with BSA as a standard (Lowry et al., 1951). Enzyme activities are expressed as μmol substrate converted (mg protein)$^{-1}$ h^{-1}.

To calculate the degree of saturation of glycolytic enzymes, the specific activity in $\mu mol.mg_{protein}^{-1}.h^{-1}$ was converted into $mmol.g_{DW}^{-1}.h^{-1}$ considering that soluble proteins represent 30% of cell dry weight. This value represents the maximal enzyme flux capacity. The *in vivo* flux in the glycolytic reactions were approximated from the glucose specific uptake rate (q_{glu}). Reactions in the top of glycolysis (hexokinase to triosephosphate isomerase) were assumed to equal the q_{glu}, while reactions in the bottom of glycolysis (glyceraldhyde-3P dehydrogenase to pyruvate kinase) were calculated as the q_{glu} times two. The degree of saturation was calculated as follows:

$$degree\ of\ saturation = \frac{approximated\ in\ vivo\ flux}{maximal\ flux\ capacity} \times 100$$

Invertase enzyme assay

The invertase assay was performed on whole cells previously described (Silveira et al., 1996). Exponentially growing cells in SMG were washed with sterile dH_2O, transferred to shake flasks (at OD 3) with 100 mL fresh SMG or SME+0.075% glucose and incubated for 2h at 30°C and shaking at 200 rpm. Afterward the dry weight of the cultures was determined and the cells were washed in 50mM sodium acetate buffer wit 50mM NaF to block the metabolism and were then suspended till a concentration of 2.5–7.5 mg dry weight per mL. 4 mL of this cell suspension were added to a dedicated vessel thermostated at 30°C, and kept under constant aeration by flushing with air (Linde, Gas Benelux, The Netherlands) and stirring with a magnetic stirrer. The reaction was started by addition of 1 mL 1M sucrose and 1 mL reaction mix was taken at 0, 1, 2, 3 and 5 min, directly filtered using 13 mm diameter 0.22 μm pore size nylon syringe filters to remove cells and put on ice. Afterward the glucose concentration resulting from sucrose hydrolysis by invertase was determined using a D-Glucose assay kit (Megazyme, Bray, Ireland). The glucose production rate was calculated in $\mu Mol \cdot min^{-1} \cdot g\ dry\ weight^{-1}$.

Staining of vacuoles

Yeast strains were stained with the red fluorescent dye FM4–64 (excitation/emission, 515/640 nm) (Thermo Fisher Scientific). Exponentially growing cells were incubated at an OD of 0.5–1 in YPD with 2 μM FM4-64 in the dark for 30 min at 30°C. Afterward cells were spun down, washed and incubated for 2–3 h in 5 mL YPD. For analysis, cells were spun down and suspended in SMG medium. Yeast cells and vacuoles were visualized with an Imager-Z1 microscope equipped with an AxioCam MR camera, an EC Plan-Neofluar 100x/1.3 oil Ph3 M27 objective, and the filter set BP 535/25, FT 580, and LP 590 (Carl-Zeiss, Oberkochen, Germany). Images were analyzed in ImageJ (NIH).

Ploidy determination by flow cytometry

Samples of culture broth (equivalent to circa 10^7 cells) were taken from mid-exponential shake-flask cultures on YPD and centrifuged (5 min, 4700g). The pellet was washed once with demineralized water, and centrifuged again (5 min, 4700g) and suspended in 800 μL 70% ethanol while vortexing. After addition of another 800 μL 70% ethanol, fixed cells were stored at 4°C until further staining and analysis. Staining of cells with SYTOX Green Nucleic Acid Stain (Invitrogen S7020) was performed as described (Haase and Reed, 2002). Samples were analyzed on a BD Accuri C6 flow cytometer equipped with a 488 nm laser (BD Biosciences, Breda, The Netherlands). The fluorescence intensity (DNA content) was represented using FlowJo (v. 10.6.1, FlowJo, LLC, Ashland, OR, USA), (Figure S15).

Transition experiment

For testing transitioning between carbon sources, strains were grown overnight in SMGal medium till mid-exponential phase. These cultures were used to plate single cells on SMG and SMGal plates (96 cells per plate) using a BD FACSAriaII (Franklin Lakes, NJ). After 5 days the percentage of cells which was growing was determined.

Whole cell lysate proteomics of humanized yeast strains

Sampling, cell lysis, protein extraction, in-solution proteolytic digestion and TMT labeling

For proteomics analysis, yeast strains grown to exponential phase in SMG shake flasks were inoculated to fresh shake flasks in biological triplicates. During mid-exponential phase samples of 8 mL were taken, centrifuged for 10 min at 5000 *g* at 4°C and the pellet was stored at −80°C. Approx. 50 mg of cell pellets (wet weight) were lysed using beads beating in 1% SDS, 100 mM TEAB, including protease inhibitor and phosphate inhibitor. The lysed cells were centrifuged and the supernatant was transferred to a new tube. The proteins were reduced with dithiothreitol and alkylated using iodoacetamide (IAA), where the protein content was precipitated and washed using ice-cold acetone. The protein pellets were dissolved in 100 mM ammonium bicarbonate buffer, and subjected to overnight digestion using proteomics grade Trypsin at 37°C and under gentle shaking using an Eppendorf incubator. The peptides were desalted using solid-phase extraction on a Waters Oasis HLB 96-well μElution plate according to the manufacturers protocol, SpeedVac dried and stored at −20°C until analyzed. One aliquot of each sample was dissolved in 3% acetonitrile in H_2O, containing 0.1% formic acid and subjected to nLC-Orbitrap-MS analysis for digestion quality control purpose. One aliquot of each sample was further dissolved in 100 mM TEAB for further labeling using a TMT 10plex labeling kit (Thermo scientific, catalog number: 90110). The peptide content of the samples were estimated using a NanoDrop photospectrometer, and the samples were diluted to achieve an approx. equal concentration. The TMT labeling agents were dissolved by adding 40 μL anhydrous acetonitrile, and 5 μL of each label was added to the individual samples. The samples were incubated at 25°C under gentle shaking, for 75 min. Then the reaction was stopped by adding diluted hydroxylamine solution, and incubated at 25°C under gentle shaking. Equal amounts of sample were combined in a LoBind Eppendorf tube. After dilution with aqueous buffer, solid phase extraction was once more performed according to the manufacturers protocol. The samples were SpeedVac dried, and stored at −20°C until analyzed. Before analysis, the samples were solubilised in 3% acetonitrile and 0.01% TFA and subjected to nLC-Orbitrap-MS analysis.

Whole cell lysate shotgun proteomics

An aliquot corresponding to approx. 500 ng of every TMT 10plex peptide mixture (SET1, SET2 and SET3, where 3 strains were mixed and compared within one SET, and each strain within one SET was present as triplicate) was analyzed by duplicate analysis employing one-dimensional shotgun proteomics. The sets were chosen to be able to directly compare the evolved strains with their parental strain and to compare the humanized strains with the *Sc*Gly strain, SET1 contained strains IMX1814, IMS0990 and IMS0991, SET2 IMX1844, IMS0987 and IMS0989, and SET3 IMX1814, IMX1844 and IMX1821. Briefly, TMT labeled peptides were analyzed using a nano-liquid-chromatography system consisting of an EASY nano LC 1200, equipped with an Acclaim PepMap RSLC RP C18 separation column (50 μm × 150 mm, 2μm and 100 Å), online coupled to a QE plus Orbitrap mass spectrometer (Thermo Scientific, Germany). The flow rate was maintained at 350nL/min over a linear gradient from 5% to 25% solvent B over 178 min, and finally to 55% B over 60 min. Solvent A consisted of H2O containing 0.1% formic acid, and solvent B consisted of 80% acetonitrile in H_2O, plus 0.1% formic acid. The Orbitrap was operated in data-dependent acquisition mode acquiring peptide signals form 385–1450 m/z at 70K resolution, 75ms max IT, and an AGC target of 3×10^6, where the top 10 signals were isolated at a window of 1.6m/z and fragmented at an NCE of 32. The peptide fragments were measured at 35K resolution, using an AGC target of 1×10^5 and allowing a max IT of 100ms.

MS raw data processing and determination of protein expression levels

For protein identification, raw data were processed using PEAKS Studio 10.0 (Bioinformatics Solutions Inc.) allowing 20 ppm parent and 0.01 Da fragment mass error tolerance, TMT10plex and Carbamidomethylation as fixed, and methionine oxidation and N/Q deamidation as variable modifications. Data were matched against an in-house established yeast protein sequence database, including the GPM crap contaminant database (https://www.thegpm.org/crap/) and a decoy fusion for determining false discovery rates. Peptide spectrum matches were filtered against 1% false discovery rate (FDR) and protein identifications were accepted as being significant when having 2 unique peptides matches minimum. Quantitative analysis of the global proteome changes between the individual yeast strains was performed using the PEAKS-Q software package (Bioinformatics Solutions Inc.), considering a quantification mass tolerance of 10ppm, an FDR threshold of 1%, using auto normalisation and ANOVA as the significance method. Significance (−10log(p)) vs fold change volcano plots were created using the scatter function in MATLAB2019b (Figures S7 and S11).

TIC normalized signal intensity was calculated by dividing the signal intensity by the total intensity of each sample (Figures S6 and S10). Mass spectrometric raw data have been deposited to the ProteomeXchange Consortium (http://proteomecentral.proteomexchange.org) via the PRIDE repository with the dataset identifier PXD025349.

Comparison human and humanized yeast glycolytic enzymes

Cell-free extract preparation and V_{max} enzyme assays

Human cells stored at −80°C were thawed, centrifuged at 20,000 *g* for 10 min at 4°C and the pellet was discarded to obtain cell-free extracts.

Yeast samples (IMX1844) were harvested as previously described (Postma et al., 1989) from exponentially growing cultures (62 mg dry weight per sample) from bioreactor. Cell-free extract preparation for yeast cells was done using YeastBuster™ Protein Extraction Reagent supplemented with 1% of 100x THP solution according to the description (Novagen, San Diego, CA, USA). To a pellet with a wet weight of 0.3 g, 3.5 mL YeastBuster and 35 μL THP solution was added. The pellet was suspended and incubated for 20 min at room temperature. Afterward the cell debris was removed by centrifugation at 20,000 *g* for 15 min at 4°C and the supernatant was used for the assays.

Prior to experimentation, YeastBuster™ Protein Extraction Reagent with 1% THP (Novagen) was added to the human cell samples and DPBS supplemented with protease inhibitor was added to the yeast samples (both as 50% of final volume). This strategy was taken in order to equalize the buffer composition of yeast and human culture samples to perform enzyme kinetics assays and proteomics.

V_{max} assays for comparison of yeast and human cell extracts were carried out with freshly prepared extracts via NAD(P)H-linked assays at 37°C in a Synergy H4 plate reader (BioTek). The reported V_{max} values represent total capacity of all isoenzymes in the cell at saturating concentrations of all substrates and expressed per extracted cell protein. Four different dilutions of extract were used to check for linearity. Unless otherwise stated, at least 2 dilutions were proportional to each other and these were used for further calculation. All enzymes were expressed as μmoles of substrate converted per minute per mg of extracted protein. Protein determination was carried out with the Bicinchoninic Acid kit (BCA Protein Assay kit, Pierce) with BSA (2 mg/mL stock solution of BSA, Pierce) as standard.

Based on the cytosolic concentrations described in literature, we have designed an assay medium that was as close as possible to the *in vivo* situation, whilst at the same time experimentally feasible. The standardized *in vivo*-like assay medium contained 150 mM potassium (Guynn et al., 1974; Rorsman and Trube, 1985; Tschopp and Schroder, 2010; Kristensen, 1986), 5 mM phosphate (Conley et al., 1997; Guynn et al., 1974), 15 mM sodium (Guynn et al., 1974; Lidofsky et al., 1993), 155 mM chloride (Breitwieser et al., 1990; Janssen and Sims, 1992), 0.5 mM calcium, 0.5 mM free magnesium (Guynn et al., 1974; Ingwall, 1982; Murphy et al., 1989) and 0.5–10.5 mM sulfate. For the addition of magnesium, it was taken into account that ATP and ADP bind magnesium with a high affinity. The amount of magnesium added equaled the concentration of either ATP or ADP plus 0.5 mM, such that the free magnesium concentration was 0.5 mM. Since the sulfate salt of magnesium was used the sulfate concentration in the final assay medium varied in a range between 0.5 and 10.5 mM. The assay medium was buffered at a pH of 7.0 (Bárány, 1996; Bruch et al., 1976; Groen et al., 1983; Ishibashi and Cottam, 1978; Oudard et al., 1996; Civelek et al., 1996) by using a final concentration of 100 mM Tris-HCl (pH 7.0). To end up with the above concentrations, an assay mixture containing 100 mM Tris-HCl (pH 7.0), 15 mM NaCl, 0.5 mM $CaCl_2$, 140 mM KCl, and 0.5–10.5 mM $MgSO_4$ was prepared.

In addition to the assay medium, the concentrations of the coupling enzymes, allosteric activators and substrates for each enzyme were as follows:

Hexokinase (HK; EC2.7.1.1) – 1.2 mM $NADP^+$, 10 mM Glucose, 1.8 U/mL glucose-6-phosphate dehydrogenase (EC1.1.1.49), and 10 mM ATP as start reagent.

Phosphoglucose isomerase (GPI; EC5.3.1.9) – 0.4 mM $NADP^+$, 1.8 U/mL glucose-6-phosphate dehydrogenase (EC1.1.1.49), and 2 mM fructose 6-phosphate as start reagent.

Phosphofructokinase (PFK; EC2.7.1.11) – 0.15 mM NADH, 1 mM ATP, 0.5 U/mL aldolase (EC4.1.2.13), 0.6 U/mL glycerol-3P-dehydrogenase (EC1.1.1.8), 1.8 U/mL triosephosphate isomerase (EC5.3.1.1), 65 μM fructose 2,6-bisphosphate as activator (synthesized as previously described (Van Schaftingen and Hers, 1981)), and 10 mM fructose 6-phosphate as start reagent.

Aldolase (ALDO; EC4.1.2.13) – 0.15 mM NADH, 0.6 U/mL glycerol-3P-dehydrogenase (EC1.1.1.8), 1.8 U/mL triosephosphate isomerase (EC5.3.1.1), and 2 mM fructose 1,6-bisphosphate as start reagent.

Glyceraldehyde-3-phosphate dehydrogenase (GAPDH; EC1.2.1.12) – 0.15 mM NADH, 1 mM ATP, 24 U/mL 3-phosphoglycerate kinase (EC2.7.2.3), and 5 mM 3-phosphoglyceric acid as start reagent.

3-Phosphoglycerate kinase (PGK; EC2.7.2.3) – 0.15 mM NADH, 1 mM ATP, 8 U/mL glyceraldehyde-3-phosphate dehydrogenase (EC1.2.1.12), and 5 mM 3-phosphoglyceric acid as start reagent.

Phosphoglycerate mutase (PGAM; EC5.4.2.1) – 0.15 mM NADH, 1 mM ADP, 2.5 mM 2,3-diphospho-glyceric acid, 5 U/mL enolase (EC4.2.1.11), 50 U/mL pyruvate kinase (EC2.7.1.40), 60 U/mL L-lactate dehydrogenase (EC1.1.1.27), and 5 mM 3-phosphoglyceric acid as start reagent.

Enolase (ENO; EC4.2.1.11) – 0.15 mM NADH, 1 mM ADP, 50 U/ml pyruvate kinase (EC2.7.1.40), 15 U/mL L-lactate dehydrogenase (EC1.1.1.27), and 1 mM 2-phosphoglyceric acid as start reagent.

Pyruvate kinase (PK; 2.7.1.40) – 0.15 mM NADH, 1 mM ADP, 1 mM fructose 1,6-bisphosphate, 60 U/mL L-lactate dehydrogenase (EC1.1.1.27) and 2 mM phosphoenolpyruvate as start reagent.

Determination of absolute enzyme concentrations [E]

Absolute concentrations of glycolytic targets was performed by targeted proteomics (Wolters et al., 2016). Isotopically labeled peptides with ^{13}C lysines and arginines were designed for human glucose metabolism and a list of peptides of interest detected in our samples can be found in Table S6.

Turnover number (k_{cat}) calculations

Turnover numbers were estimated based on the equation $V_{max} = k_{cat} \cdot [E]$, the maximal enzyme activity was divided by the concentration of each individual peptide detected by proteomics when no other isoform was detected. In the human skeletal muscle samples, more than one isoform was detected for certain proteins. In these cases (phosphoglycerate mutase, enolase and pyruvate kinase) the sum of the concentrations of all isoforms was used to estimate the turnover number. In Figure S13 k_{cat} values were calculated for the specific isoforms based on the ratio between turnover numbers found in the literature for the human isoforms. Protein concentrations [E] were measured as $pmol \cdot mg\ protein^{-1}$ and V_{max}'s as $\mu mol \cdot min^{-1} \cdot mg\ protein^{-1}$. In order to obtain k_{cat} values in min^{-1}, the following equation was used for each enzymatic reaction in the dataset:

$$k_{cat} = \frac{V_{max}}{[E]} \cdot 10^6$$

QUANTIFICATION AND STATISTICAL ANALYSIS

Statistical analysis was performed in Graphpad Prism and Microsoft Excel. K_m and IC_{50} estimations were performed in Graphpad Prism. Statistical details (number of replicates and used tests) of experiments can be found in the figure legends. Significance was usually defined by p values < 0.05.